J. Fluid Mech. (1991), *vol.* 225, *pp.* 575–606
Printed in Great Britain

On the evolution of a wave packet in a laminar boundary layer

By JACOB COHEN[1], KENNETH S. BREUER[2] AND JOSEPH H. HARITONIDIS[2]

[1] Faculty of Aerospace Engineering, Technion – Israel Institute of Technology, Haifa 32000, Israel

[2] Department of Aeronautics and Astronautics, Massachusetts Institute of Technology, Cambridge, MA 02139, USA

(Received 12 July 1990)

The transition process of a small-amplitude wave packet, generated by a controlled short-duration air pulse, to the formation of a turbulent spot is traced experimentally in a laminar boundary layer. The vertical and spanwise structures of the flow field are mapped at several downstream locations. The measurements, which include all three velocity components, show three stages of transition. In the first stage, the wave packet can be treated as a superposition of two- and three-dimensional waves according to linear stability theory, and most of the energy is centred around a mode corresponding to the most amplified wave. In the second stage, most of the energy is transferred to oblique waves which are centred around a wave having half the frequency of the most amplified linear mode. During this stage, the amplitude of the wave packet increases from 0.5% to 5% of the free-stream velocity. In the final stage, a turbulent spot develops and the amplitude of the disturbance increases to 27% of the free-stream velocity.

Theoretical aspects of the various stages are considered. The amplitude and phase distributions of various modes of all three velocity components are compared with the solutions provided by linear stability theory. The agreement between the theoretical and measured distributions is very good during the first two stages of transition. Based on linear stability theory, it is shown that the two-dimensional mode of the streamwise velocity component is not necessarily the most energetic wave. While linear stability theory fails to predict the generation of the oblique waves in the second stage of transition, it is demonstrated that this stage appears to be governed by Craik-type subharmonic resonances.

1. Introduction

The transition from a laminar to a turbulent state in open flows, such as boundary layers, is a process by which disturbances of infinitesimal amplitude level (of the order of 0.1% of the mean velocity or less) grow to amplitude levels in excess of 30% of the mean velocity. This process is commonly addressed from the stability viewpoint. In the initial stages, it can be characterized through the growth of small two-dimensional disturbances with downstream distance (linear instability). At later stages, it continues through a nonlinear deterministic regime where the waves develop a three-dimensional configuration, distort the mean flow, generate higher harmonics, and finally break down into turbulence.

The growth of small two-dimensional wavy disturbances in a laminar flow over a flat plate was predicted by the theoretical work of Tollmien (1929) and subsequently

verified in the experiments of Schubauer & Skramstad (1947). They measured the growth rates and propagation velocities of periodic two-dimensional waves excited artificially by an oscillating ribbon. The results were in substantial agreement with the linear stability calculations for parallel mean flow done by Schlichting (1933). These waves grow with downstream distance and, after achieving a certain amplitude, develop a three-dimensional configuration with periodicity in the spanwise direction, as seen in the experiments by Klebanoff, Tidstrom & Sargent (1962). Finally, the entire boundary layer becomes turbulent.

The nonlinear mechanism describing the secondary growth of three-dimensional waves has been the subject of intensive theoretical investigations. Benney & Lin (1960) considered only the induced mean flow resulting from the non-resonant interaction between two- and three-dimensional waves. Although the model reveals a secondary system of spanwise-periodic longitudinal vortices which are qualitatively similar to those reported by Klebanoff *et al.* (1962), it was criticised by Stuart (1962) because of the difference in wave speeds between the two- and three-dimensional waves, in contradiction to the observations. The first theoretical approach to be confirmed experimentally was due to Raetz (1959, 1964), who showed the possibility of resonant wave triads in the boundary layer although he restricted his analysis to neutrally stable two-dimensional waves. This approach was extended to include non-neutral waves in general parallel shear flows by Craik (1971). Although this mechanism, which assumes a small-amplitude two-dimensional primary wave, did not explain the results of Klebanoff *et al.* (who used a high level of excitation of the fundamental frequency), this subharmonic growth was observed experimentally by Saric & Thomas (1984) and Kachanov & Levchenko (1984) both of whom used a low level of excitation. Herbert (1984) analysed the secondary instability problem by considering the mean flow to be composed of the Blasius profile with a saturated finite-amplitude two-dimensional wave. Using Floquet theory, he found that there exists a broadband, three-dimensional, instability mechanism, strongly dependent on the amplitude of the two-dimensional primary wave. As a special case, the Craik-type resonance is recovered as the amplitude of the primary wave goes to zero. Calculations based on this theory agree very well with the available experimental data (cf. Herbert 1988; Corke & Mangano 1989).

On the basis of resonance theory, Itoh (1987) showed that the existence of two-dimensional waves with finite amplitude can induce three-dimensional distortion with spanwise periodicity in the mean flow. The interaction of the distorted mean field with Tollmien–Schlichting waves yields new three-dimensional travelling waves, with the same streamwise wavenumber as the two-dimensional waves, and with the same spanwise wavenumber as the mean flow.

The early stages of natural transition do not involve a single mode, but have a wide spectrum of modes, resulting from either broadband free-stream turbulence or a localized initial disturbance. In order to simulate this more natural situation, Gaster & Grant (1975) used a pulse excitation rather than a periodic wave maker. In this way, all possible modes are excited and a wave packet is formed through selective amplification and interference of the linear waves. By positioning a single hot wire just outside the laminar boundary layer, Gaster & Grant followed the evolution of a wave packet from a smooth packet having a single amplitude maximum close to the centreline to a distorted pattern further downstream having two amplitude maxima on either side of the centreline.

The 'linear' stage of the evolution was successfully compared to the theoretical model proposed by Gaster (1975) who described a wave packet as a superposition of

the least-stable mode of all two- and three-dimensional waves. Asymptotic theory has also been applied to determine the linear wave packet's downstream evolution and despite some early differences in the correct evaluation of the asymptotic integral and the predicted shape of the wave packet far downstream from the point of generation (see, for example, Benjamin 1961; Criminale & Kovasznay 1962; Gaster 1968) the more recent work by Gaster (1982*a*, *b*) and by Craik (1981) appears to have resolved these problems. Regarding the nonlinear evolution of wave packets, a weakly nonlinear asymptotic theory for marginally unstable two-dimensional wave packets was presented by Stuartson & Stuart (1971), and some brief results for the nonlinear three-dimensional wave packet have been reported by Itoh (1984). Nevertheless, this theory is still incomplete.

Morkovin (1969) pointed out that the traditional Tollmien–Schlichting route to transition might be bypassed directly by nonlinear effects when the initial amplitude of the disturbances is sufficiently high to perturb the base flow. This was investigated by Amini & Lespinard (1982) who initiated an 'incipient spot' in the boundary layer by means of an air jet through a small hole in the wall. A more extensive study which demonstrated the linear and nonlinear mechanisms that may contribute to the bypass mechanism was conducted by Breuer & Haritonidis (1990) and Breuer & Landahl (1990) who considered localized disturbances in general. Their measurements and computations show that any three-dimensional initial disturbance may be described in terms of a wave part, and a 'transient' part which derives from the excitation of vertical vorticity modes by the initial disturbance field. While the wave part of the disturbance is that part governed by linear stability theory and studied by Gaster (1975), the transient portion of the disturbance develops into an inclined shear layer which intensifies and elongates with time, in accordance with the theoretical predictions of Landahl (1975, 1980) who showed that any general three-dimensional disturbance may be subjected to an algebraic instability. However, if the initial disturbance amplitude is sufficiently small, the transient initially grows, but will eventually decay, leaving only the linear wave portion at downstream locations. In the present work, the transient part of the initial disturbance, while present, has decayed sufficiently, and does not play any dynamical role in the disturbance evolution.

The overall purpose of the work reported here was to follow the evolution of localized disturbances in a laminar boundary layer from a low-amplitude wave packet to the formation of a turbulent spot. To the best of our knowledge this is the first time that all the stages have been recorded in one experiment. The present work extends the previous experimental investigation done by Gaster & Grant (1975) which was concerned with the initial stages of formation and growth of a wave packet where the amplitudes are generally insufficient to generate significant nonlinear distortion of the boundary layer. Here, the main focus is on the transition stages, and in particular where nonlinear effects are significant. While in previous investigations only the streamwise velocity component was measured at a single vertical location just outside the boundary layer, in the present work the entire spatial structure of the disturbed flow field is mapped by hot-wire measurements which include all three velocity components.

2. Experimental arrangement

2.1. *Description of the apparatus*

The experiments reported here were done in the closed-loop low-turbulence wind tunnel in the Turbulence Research Laboratory at MIT. The test section is 6.1 m long, 1.22 m high and 0.6 m wide. The flat plate, made of aluminium, is 12.7 mm thick and is mounted vertically, 10 cm from one of the tunnel sidewalls. A tapered leading edge with a rounded tip is attached to the front of the plate. The plate extends the entire length of the test section and to within 10 cm of both the tunnel floor and ceiling. The plate is joined to the floor and ceiling by a porous metal plate behind which are ducts for suction of the boundary layers which grow in the corners of the test section. The suction control was successfully used to contain the contamination by the corner flows and to maintain a high-quality laminar boundary layer over the central span of the flat plate.

A right-handed coordinate system is defined with x, y, z as the downstream, vertical (wall-normal), and spanwise (parallel to the wall) directions respectively, with U, V and W being the corresponding velocity components. Note that in the discussion, the term 'vertical' always refers to the direction normal to the wall, regardless of the actual orientation of the apparatus in the laboratory. The measurements cover a 350 cm distance along the x-direction and ± 40 cm in the z-direction. In the initial, exploratory measurements, the wave packet was generated with a circular membrane, similar to the one used by Breuer & Haritonidis (1990). However, the disturbance generated in this manner proved to be unsatisfactory since the transient portion was too large. A more successful method was used by which the disturbance was generated by a controlled, sinusoidal, air pulse which was introduced into the boundary layer through a circular, perforated disk. The perforations, 0.5 mm in diameter, were confined within a circle of 0.5 cm diameter located on the centreline of the plate, at a downstream distance of $x_0 = 81$ cm from the leading edge. The sinusoidal air pulse was generated by a loudspeaker mounted at the back of the plate and connected to the cavity behind the perforated disk through a flexible tube, 7 cm long and having an inner diameter of 0.5 cm. The speaker was driven from the amplified output of a function generator.

The free-stream velocity, U_0, used in the experiments was 6.65 m/s, so that the local Reynolds number (based on displacement thickness, δ_1) at the location of the disturbance generator was approximately 1000. The excitation signal to the speaker was a single period of a 24 Hz sinusoid. This particular frequency was chosen so that the corresponding two-dimensional wave just becomes unstable, according to linear stability theory, at the location of the disturbance generator. In the experiments reported here, two sets of data were obtained under the same conditions except that the initial amplitude level of the wave packet was higher in the second set of measurements. The measurements are dense along the x- and z-coordinates and include a y-mapping of the flow field.

The flow measurements were made using constant-temperature hot-wire anemometry. The streamwise and spanwise velocity components were measured with a V-shaped hot-wire probe while the vertical velocity component was obtained by using a standard $\times$-probe. The hot wires, made using Wollaston wire 1.27 μm in diameter, were built in-house and had a length-to-diameter ratio greater than 300; they were operated at a resistive overheat of 30% and had a maximum frequency response of 30 KHz as determined through the square-wave technique.

The data was acquired using a Phoenix Data A/D system connected to a PDP

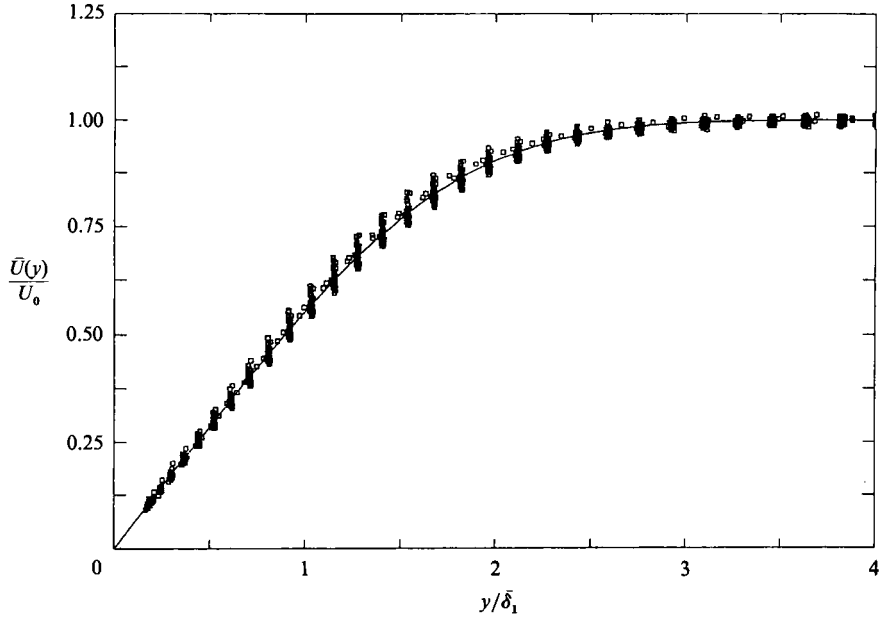

FIGURE 1. Velocity profiles measured at 78 locations at $x = 50$ to 350 cm in 25 cm intervals, and at $z = \pm 5$, ± 20, and ± 40 cm. The solid line represents the Falkner–Skan solution with a wedge angle parameter value of $\sigma = 0.01$.

11/55 computer. In addition, the computer controlled the positioning of the probe via stepping motors as well as the timing of disturbance generation. Additional processing and data acquisition were performed with a Microvax II computer.

2.2. *Mean flow characteristics*

Two criteria were used to determine the quality of the flow in the test section: the uniformity of the boundary layer across the span of the plate, and the extent to which the flow conformed to a Blasius boundary layer. The spanwise uniformity was characterized by measuring the displacement thickness, δ_1, at 1 cm intervals over a span of 80 cm at different x-locations. The deviation of the displacement thickness was less than $\pm 5\%$ of the mean value at $x = 100$ cm and at free-stream velocity of 10.3 m/s, except for the locations at $z = 10$, -2 and -12 cm where the deviation was 6, 7 and 10% respectively. It should be emphasized that these deviations are very sparsely distributed (3 out of 81 locations), are very localized (with a spanwise extent of less than 1 cm) and did not have any measurable effect on the evolution or structure of the wave packet. Moreover, no significant asymmetries were observed in the measurements, even though the locations of the peaks are not symmetric about the centreline.

The development of a small-amplitude wave packet to a spot at such a free-stream velocity requires a long downstream distance (3.5 m) and a wide spanwise spread (80 cm). Seventy eight velocity profiles are plotted in figure 1 and are compared with a Falkner–Skan profile, given by the solid line, with a wedge angle parameter value of σ equal to 0.01 (note: the Falkner–Skan parameter is often denoted by the symbol β. However, in this paper, β is used to represent the non-dimensional frequency and so in order to avoid confusion, the Falkner–Skan parameter is represented here by σ). The deviation of the measured profiles from the Blasius profile was the result of a slightly accelerating flow. The profiles were measured at 13 downstream stations

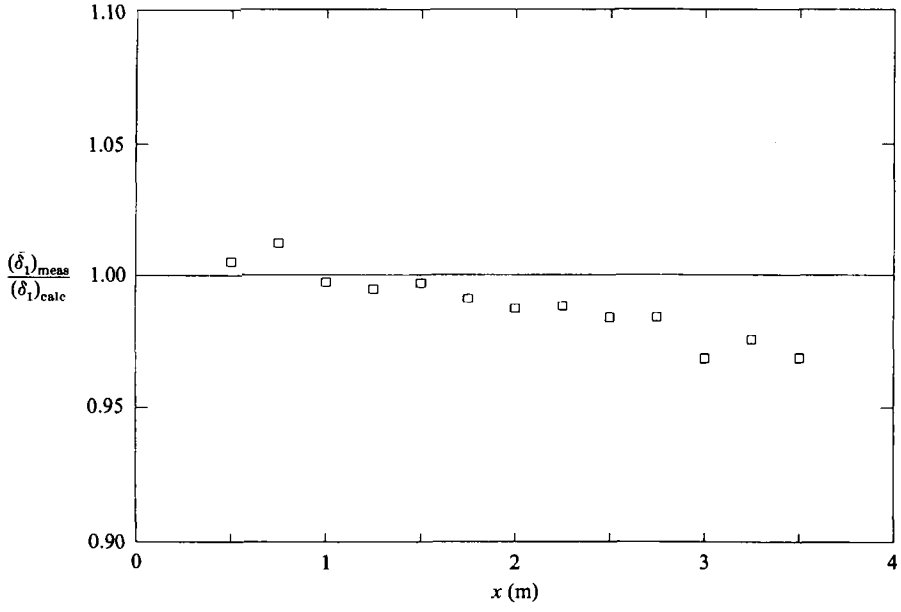

FIGURE 2. The downstream development of $\bar{\delta}_1$ normalized to δ_1 computed for a Falkner–Skan profile with a wedge angle parameter value of $\sigma = 0.01$.

from $x = 50$ cm to 350 cm in 25 cm intervals, and at the six z-locations of ± 5, ± 20, and ± 40 cm. All profiles were normalized using the same virtual origin and, at a given downstream distance, by the average displacement thickness of all six profiles at that location. The deviations from the Falkner–Skan profile do not show any consistent trend, so one may infer that they are due to either experimental error or slight differences in the corner suction, used to contain the spreading of turbulence from the corner flows. The latter possibility seems the most likely one as the deviations of profiles spanning $z = \pm 20$ cm are considerably smaller than those at ± 40 cm. In figure 2, the downstream evolution of the measured average displacement thickness, $\bar{\delta}_1$, is compared with the displacement thickness calculated for the Falkner–Skan profile. By comparing the computed amplification rates of linear disturbances in a Blasius flow with those in a Falkner–Skan flow (with $\sigma = 0.01$), we find that the stability characteristics of the present flow are slightly altered with the maximum amplification rate decreasing by approximately 12% at $Re = 1500$ (the Reynolds number corresponding to $x = 170$ cm).

While the mean flow is accelerating slightly, profiles at any x-location fit the Blasius profile very well when normalized by local parameters, i.e. U_0 and δ_1. Amplitude equations will naturally depend on the total flow history, in which case the slight acceleration of the mean flow will have to be taken into account. Since the present results depend on local quantities only, we opted, for simplicity, to work with the Blasius profile.

2.3. *Experimental procedure and data processing*

The disturbed flow field, generated by the air pulse, was mapped by positioning the hot-wire probe at an (x, y, z) location downstream of the disturbance generator and measuring the velocity trace as the disturbed flow was advected past the probe. The positioning of the probe within the boundary layer at a given downstream station

was done automatically by using the computer to drive the stepping motors and taking advantage of knowing the profile shape. First, the probe was moved, in accordance with the local Blasius solution, to a desired y-location where $U(y)/U_0$ had a certain value. Then, in order to position the probe more precisely, an iterative interpolation scheme was performed until a specified accuracy, typically within a $\pm 2\%$ deviation from the desired value of $U(y)/U_0$, was achieved.

The measurement sequence was initiated by a pulse from the computer which triggered the disturbance generator. After waiting a delay time, $T_0 = (x-x_0)/0.935U_0$, the velocity record, consisting of 512 points, was digitized at a rate such that the total non-dimensional measuring time, $\tau = (T-T_0)\,U_0/(x-x_0)$, was approximately 3. The values of the delay time and total measuring time were based on the propagation velocities of the wave-packet leading and trailing edges, found by Gaster & Grant (1975) to be 0.44 and 0.36 of U_0 respectively. The total measuring time and the number of points in a velocity record provided sufficient information to capture all the relevant frequencies associated with the wave packet.

At each measuring point, N events (realizations) of the disturbance's passage were recorded and an ensemble average was then formed. The number of events, N, was a function of the amplitude of the measured disturbance. For very weak disturbances, having a streamwise perturbation amplitude of less than 0.2% of U_0, 200 events were measured, while for very strong disturbances, having a streamwise perturbation amplitude of more than 10% of U_0, 30 events were sufficient to accurately represent the structure. In order to further reduce high-frequency noise, digital filtering was performed on the ensemble-averaged signal. Unless noted differently, the filtering frequency corresponds to the non-dimensional frequency, $\beta = 2\pi f\delta_1/U_0$, of 0.4.

The fluctuation velocities, denoted by the lower-case letters u, v and w, were obtained by subtracting the local mean from the ensemble signal. Typically, the disturbance occupied one third of the total measuring time of each signal record. When ensemble averaged and filtered, the signals were almost indistinguishable from individual realizations in the linear and subharmonic stages so that the spectra of these signals are a true representation of the spectral content of the individual events. The signal averaging was done to eliminate low frequencies caused by occasional probe vibration and free-stream velocity fluctuations, while the digital low-pass filtering was done to eliminate high-frequency oscillations (e.g. electrical noise).

The Fourier decomposition was accomplished using fast Fourier transforms (FFTs) when only a single transform of the time domain was needed. However, for a double Fourier transform of both the time and spanwise domains, a combined procedure which included a FFT in the time domain and a direct Fourier transform in the spanwise domain was performed. This procedure was needed since the spanwise structure of the disturbance grows with downstream distance and it was difficult to keep a good and consistent resolution in the spanwise direction when the number of points in the Fourier transform was restricted to be an integer power of 2. The power spectral densities were smoothed by applying Hanning weights in which each discrete density is represented by the sum of half of its original value and a quarter of the power of each one of its two neighbouring densities.

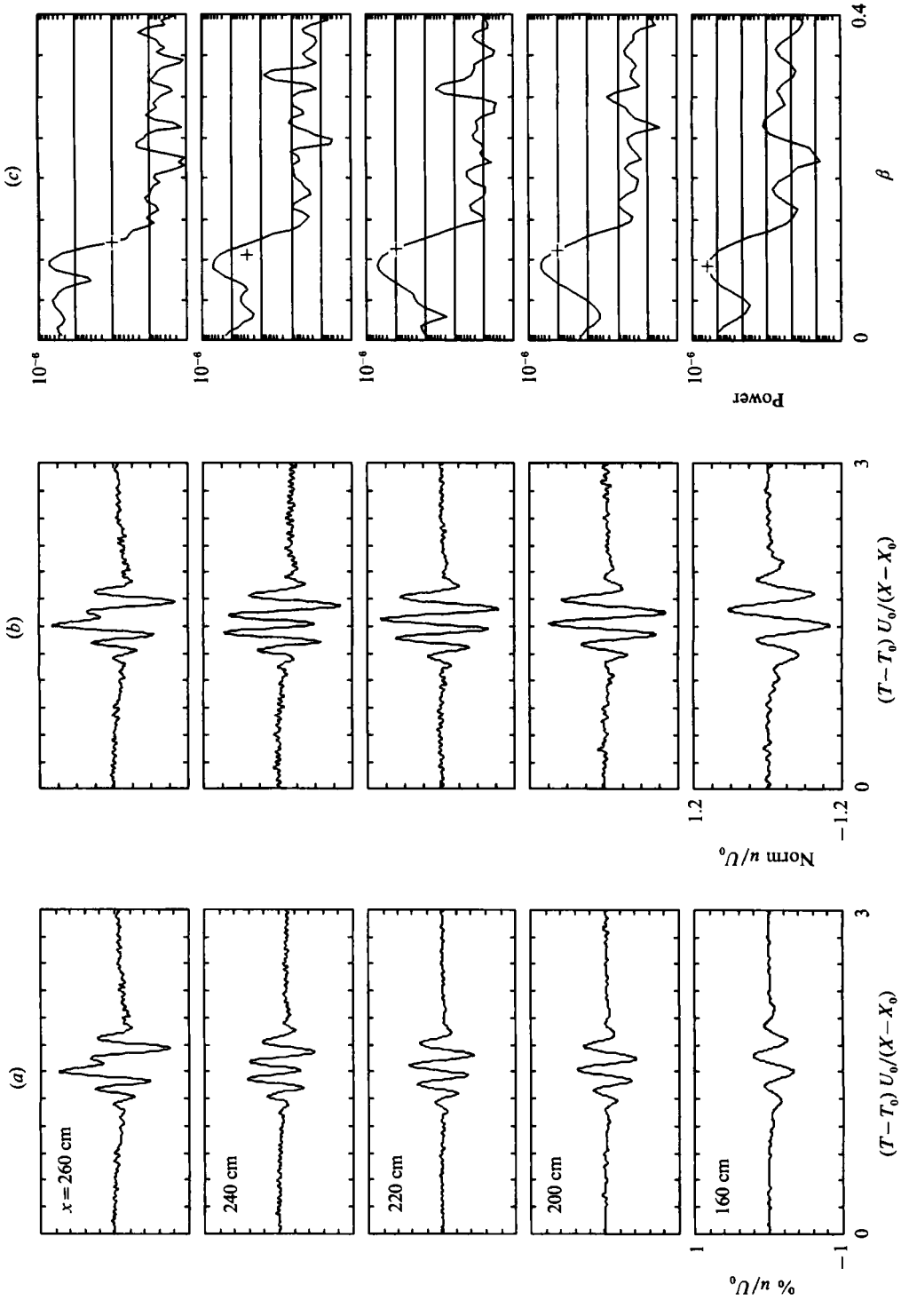

FIGURE 3. For caption see facing page.

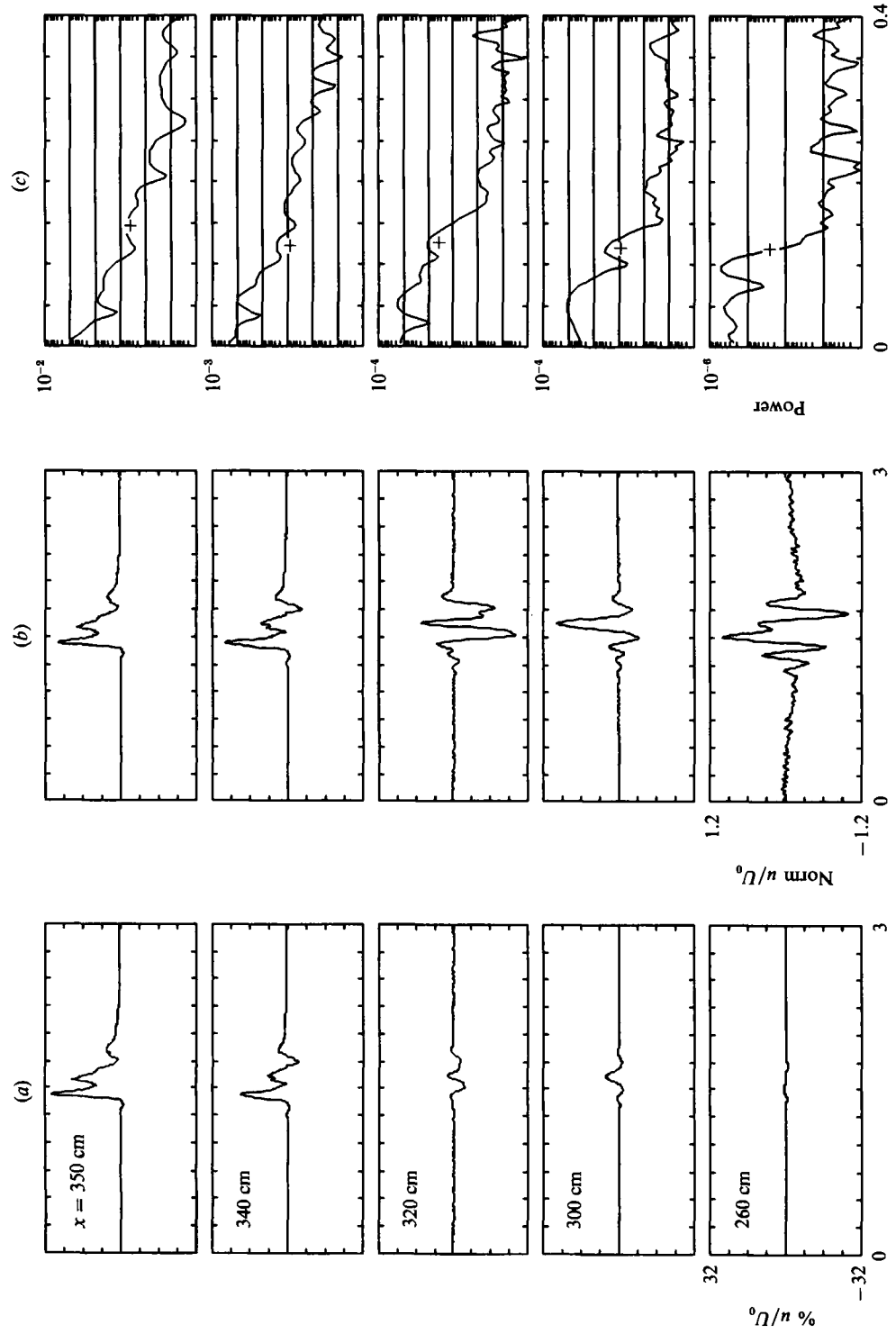

FIGURE 3. Downstream development of the wave packet along the centreline and at $y/\delta_1 = 0.62$ shown by a set of ensemble averages of (*a*) streamwise fluctuation records normalized by the free-stream velocity; (*b*) normalized signals displaying the same maximum amplitude for all downstream locations; (*c*) associated power spectra of the ensemble-averaged signals.

3. Results and discussion

3.1. *Experimental observations*

The following results describe the temporal and spatial evolution of a controlled localized disturbance in a laminar boundary layer from a low-amplitude wave packet to the formation of a turbulent spot. By low-amplitude wave packet, it is meant, firstly, that the amplitudes are small enough so that it can be considered to be a superposition of all waves which grow initially according to linear stability theory, as was shown by Gaster (1975). Secondly, it is meant that the amplitude of the transient portion of the initial disturbance, which is concentrated in the very low frequencies of the disturbance spectrum, is not too large and has substantially decayed through viscous diffusion by the time the disturbance reaches the first measuring station.

The development of the wave packet with increasing downstream distance is shown in figure 3. Measurements were made at several downstream stations, along the centreline, and inside the boundary layer where the mean velocity is 35% of the free-stream velocity. This particular y-location, whose dimensional distance from the plate varies with downstream distance, was chosen because it corresponds approximately to the location at which the streamwise fluctuation of the most-amplified two-dimensional wave attains its maximum according to linear stability theory.

In figure 3(a), the plots are normalized by the free-stream velocity, while in figure 3(b) the plots have been normalized to display the same maximum fluctuations. By using these scalings, both the amplification of the wave packet and its detailed shape can be observed. Figure 3(c) shows the associated power spectrum distributions versus the non-dimensional frequency, $\beta = 2\pi f \delta_1 / U_0$. Since the relevant scales are the local displacement thickness of the boundary layer, δ_1, and the free-stream velocity, U_0, these were used to render the frequency dimensionless. Owing to the dispersion relationship of the waves within the wave packet, both the leading and trailing edges of the wave packet travel at constant but different velocities. This results in the spread of the signal in time being proportional to the distance travelled. The divergence of the flow can be appreciated by following the dimensional frequency of 30 Hz which corresponds to $\beta = 0.093$ at $x = 160$ cm and to $\beta = 0.138$ at $x = 350$ cm. The values of β corresponding to the dimensional frequency of 30 Hz have been indicated at the various downstream distances with small crosses marked on the associated power spectra plots.

Three stages of transition are observed. In the first stage (referred to as the linear stage) the wave packet can be treated as a superposition of two- and three-dimensional waves governed by linear stability theory (see Gaster & Grant 1975; Gaster 1975). In this experiment, the linear stage is observed from $x = 160$ cm to 220 cm, where most of the energy is centred around a wave of frequency $\beta = 0.1$, corresponding to the most amplified wave (for these Reynolds numbers) according to linear stability theory (Jordinson 1970). The amplitude of the wave packet is very low, 0.3% of U_0 at $x = 160$ cm and 0.46% at $x = 220$ cm. During this stage, the transient part of the initial disturbance, which is concentrated in low frequencies, decays through viscous diffusion. In the second stage (referred to as the subharmonic stage) waves centred around $\beta = 0.05$ begin to gain energy. This stage starts at $x = 220$ cm and continues to develop up to $x = 300$ cm, where the subharmonic band of waves overtakes the fundamental band, and the wave packet loses one of its fundamental periods (see figure 3a, $x = 260$ cm). The amplitude of the wave packet

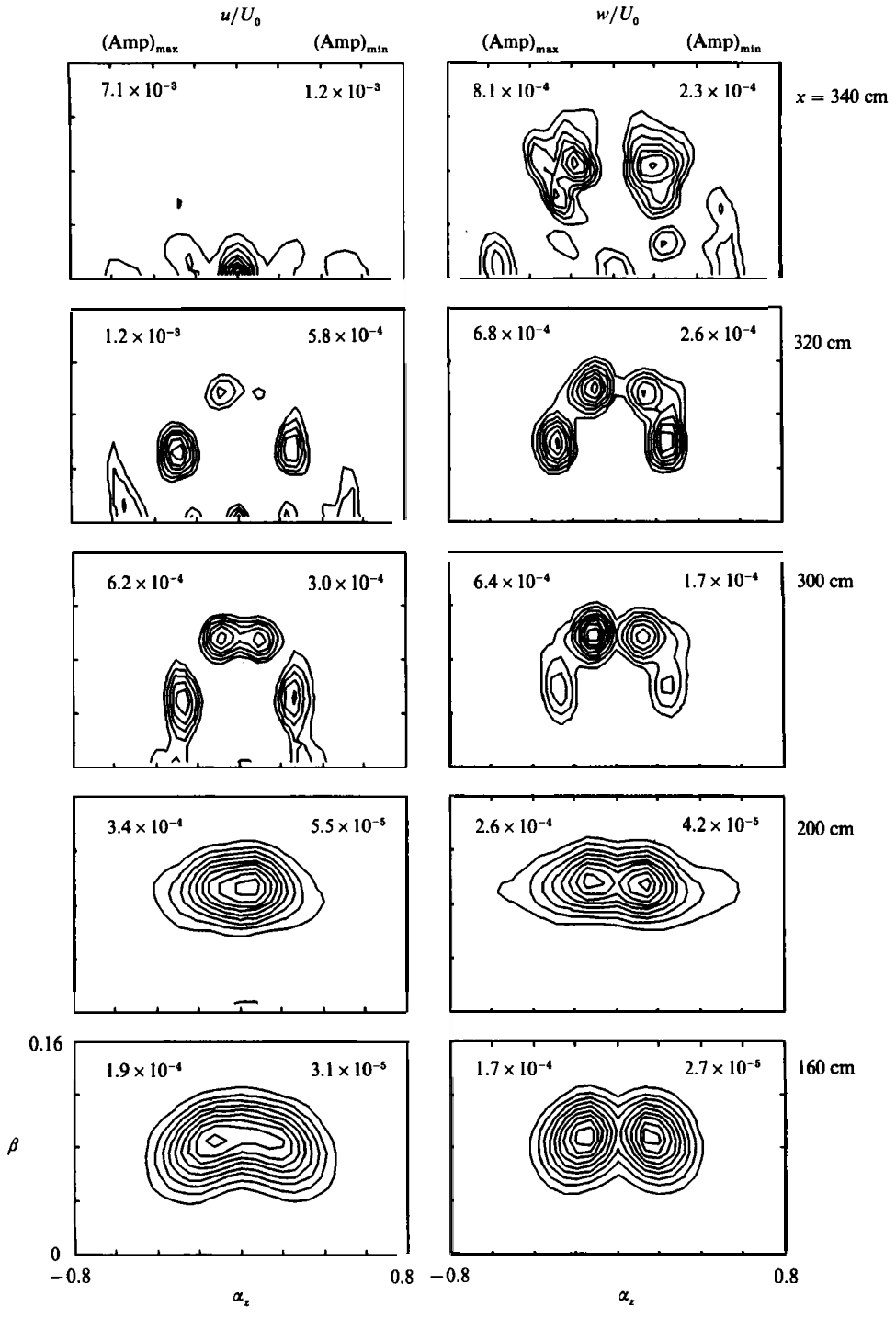

FIGURE 4. Spanwise wavenumber versus frequency spectra of streamwise and spanwise ensemble-averaged velocity fluctuation signals at different downstream locations and at $y/\delta_1 = 0.62$.

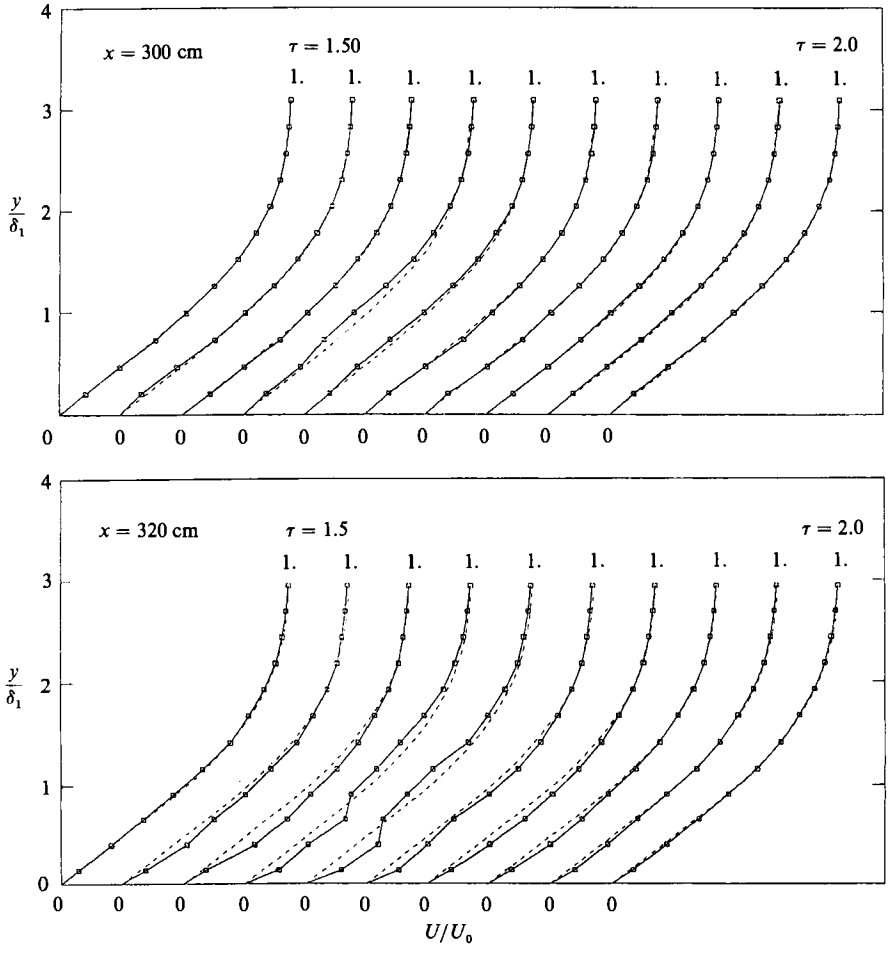

FIGURE 5. Subharmonic stage at $x = 300$ and 320 cm and $z/\delta_1 = 15.0$. Ensemble average of instantaneous velocity profiles at various passage times of the disturbance. The symbols, connected by a solid line, represent the measured profile while the dotted line indicates the calculated Blasius profile.

within this stage increases from 0.47% of the free-stream velocity at $x = 240$ cm to 5.2% at $x = 300$ cm. During the final stage, which is observed between $x = 320$ cm and 350 cm, a turbulent spot develops. This stage starts with an increase of energy at low frequencies of the wave packet ($x = 320$ cm) and then a rapid increase at high frequencies ($x = 340$ cm), followed finally by an apparent sharp increase at low frequencies which results in a signal that is at all times positive and of very high amplitude (27% of the free-stream velocity). At this point, ensemble averages are no longer representative of individual realizations because of the loss of coherence between the various scales present.

Measurements of the U and W velocity components in the (x, z)-plane and at a y-location where $U/U_0 = 0.35$ enable us to calculate the wavenumber–frequency spectra of U and W at several downstream locations (figure 4). In the linear stage, at $x = 200$ cm for example, the wave having the highest amplitude has a non-dimensional frequency of 0.09 and a zero non-dimensional (with respect to δ_1) spanwise wavenumber (α_z), i.e. it is a two-dimensional wave. The two-dimensional component of the normal velocity, v, is the most amplified and consequently the

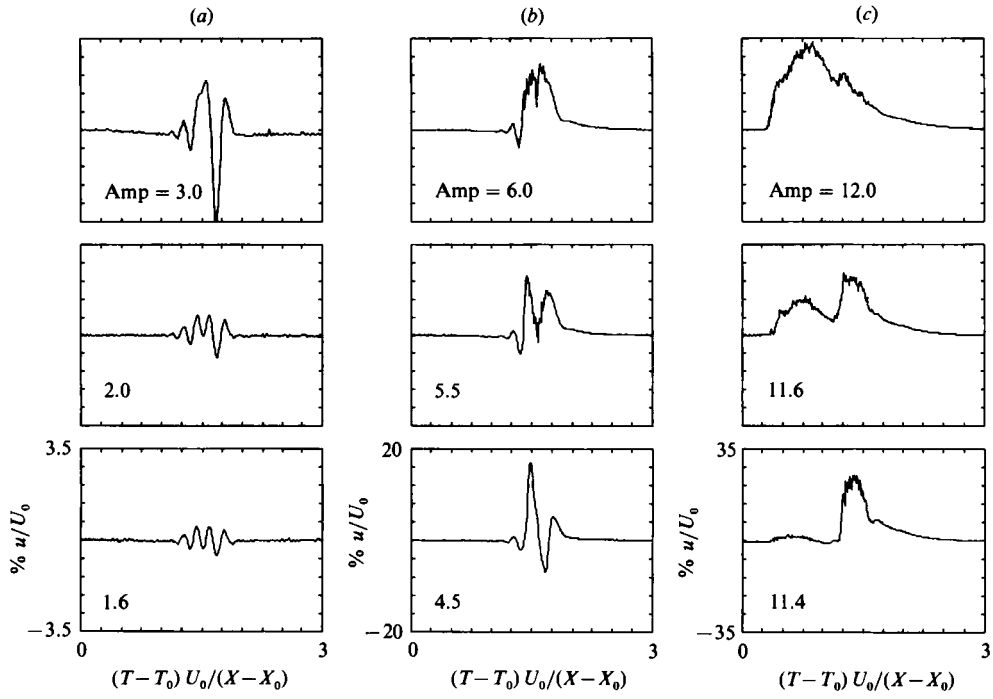

FIGURE 6. The development of the wave packet with increasing speaker amplitude at a fixed downstream distance. Hot wire is located at $x = 240$ cm, $z = 0$, and at $y/\delta_1 = 0.62$.

most energetic one. However, owing to the contribution of the vertical vorticity, the behaviour of the vertical component, v, is not necessarily reflected by the other two components, u and w. This statement, which is supported experimentally by the two-dimensional power spectra at $x = 160$ cm, will be discussed in more detail in §3.2. The two-dimensional spectra at $x = 300$ cm clearly show that in the subharmonic stage two bands of symmetric oblique waves are formed. In the third stage, spectral peaks representing different sums and differences of the primary and subharmonic peaks can be observed. For example, at $x = 320$ cm a peak at $\beta = 0$, $\alpha_z = 0$ has emerged from the interaction between the primary peak and the two subharmonic peaks. Finally, at $x = 340$ cm, there is a rapid increase of energy at both very low frequencies and spanwise wavenumbers.

Ensemble averages of the instantaneous velocity profiles at the early ($x = 300$ cm) and late ($x = 320$ cm) subharmonic stages at $z/\delta_1 = 15.0$ are shown in figure 5. The measured profiles are compared with the Blasius velocity profile indicated by the dotted lines. The velocity distributions at the leading and trailing edges of the wave packet do fit the profile; however, the rest of the profiles are distorted. Some of the profiles have inflexion points which may lead to an inviscid Rayleigh instability producing the high frequencies that we observe immediately after this stage. The formation of internal shear layers and their subsequent breakdown has been previously observed (for example, the 'spike' stage described by Klebanoff *et al.* 1962). Inflexional profiles were also seen on the centreline but were not as pronounced.

In order to follow more carefully the nonlinear stage, the idea that an increase in the initial amplitude level of the wave packet should shorten the linear stage and thus advance the entire transition process further upstream was used. In figure 6, the

signals of the streamwise fluctuations are measured at a fixed x-location of $x = 240$ cm, at a y-location where $U/U_0 = 0.35$ and for several values of the speaker amplitude. The value of the speaker amplitude is an arbitrary (not necessarily linear) measure of the amplitude of the initial disturbance. In figure 6(*a*) the subharmonic stage, where the subharmonic waves take over and the signal loses one of its fundamental periods, is recovered by increasing the speaker amplitude from 1.6 to 3.0. At a level of 4.5, low- and high-frequency waves gain energy, and at a speaker level of 5.5 the formation of the spot begins.

At higher excitation levels, the disturbance measured at $x = 240$ cm continues to grow, gaining energy at both high and low frequencies. At an amplitude level of 11.4, a secondary bulge appears in front of the leading edge of the spot and at even higher levels of initial excitation the two bulges merge into a single spot.

For all amplitude levels up to $A = 8$, the velocity traces at $x = 240$ cm were the same as the traces eventually observed at some downstream distance in the first series of measurements, where the speaker amplitude was very small. From this we conclude that increasing the speaker amplitude did not result in any observable difference in the transition process other than advancing the entire process upstream and shortening the linear stage. For amplitudes greater than $A = 8$, the secondary bulge in the measured velocity at $x = 240$ cm was not observed at any location in the low-amplitude series, indicating that it is not a natural consequence of the wave packet's growth, but rather it is associated with the initial disturbance generation. Breuer & Haritonidis (1990) have shown that for low amplitudes of the initial disturbance, the transient decays exponentially. However, as the initial disturbance becomes more energetic (Breuer & Landahl 1990), the transient can grow and the distortion in the disturbance that we observe here may be due to such a contamination from the nonlinearly growing transient.

In all subsequent measurements, a higher initial amplitude was used so that the nonlinear stages could be easily observed. In this series, the three characteristic stages of transition, linear, subharmonic and turbulent spot were observed at the earlier x-locations of $x = 170$, 230 and 270 cm. (Corresponding approximately to $x =$ 200, 270 and 360 cm in the original low-amplitude series.) The streamwise velocity and its associated power spectrum at these new locations is shown in figure 7. The measurements were made on the centreline and inside the boundary layer, where the local velocity was 35% of the free-stream velocity. In addition, the streamwise signal and its spectrum at $x = 260$ cm is shown. This location (corresponding to $x = 320$ cm in the low-amplitude series) represents the beginning of the spot formation process. Despite the high fluctuation amplitudes (15% of U_0) the velocity signals at this stage are still coherent and the spectrum of the ensemble is thus still meaningful. Although the signal at the turbulent spot stage ($x = 270$ cm) is no longer coherent, the presence of high frequencies is evident, indicating the rapid breakdown of the disturbance that has taken place in the short distance from $x = 260$ to 270 cm. Recalling figure 5, in which inflexional velocity profiles were observed at the equivalent x-location, it seems very likely that the generation of the high frequencies observed here is associated with the breakdown of those distorted profiles due to inflexional instabilities.

The two-dimensional spectra associated with the first three of these four stations are shown in figure 8. Comparison with the corresponding two-dimensional spectra in figure 4 emphasizes again the fact that when the initial amplitude level of the wave packet is increased its spatio–temporal structure remains unchanged through the various stages of transition except for a shift in the x-coordinate. However, since the

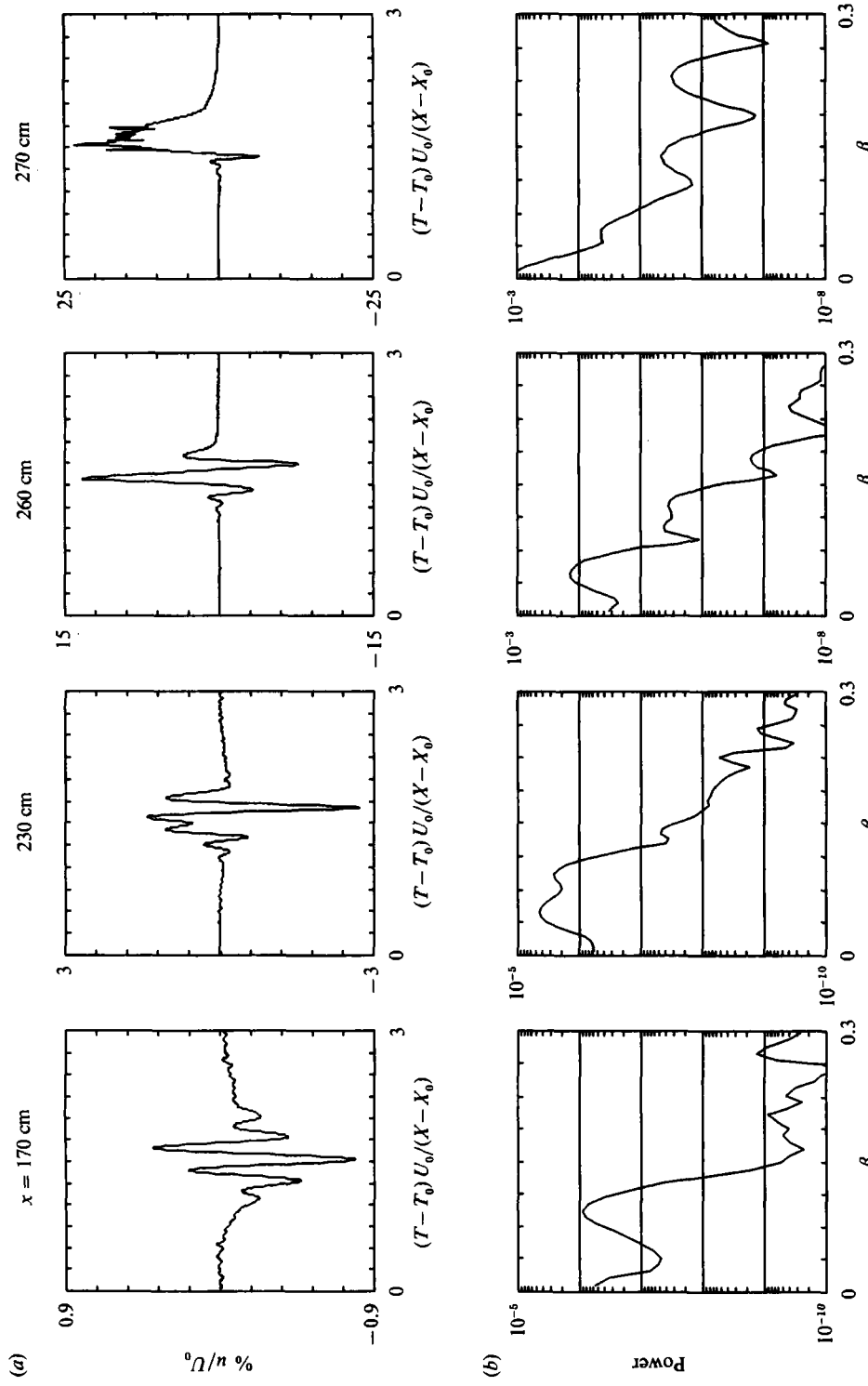

FIGURE 7. Four stages of the transition process: a small-amplitude wave packet, the subharmonic stage, the post-subharmonic stage and the turbulent spot stage are shown by (*a*) ensemble averages of the streamwise velocity fluctuations measured along the centreline at $y/\delta_1 = 0.62$ and at the representative downstream locations, and (*b*) their associated power spectra.

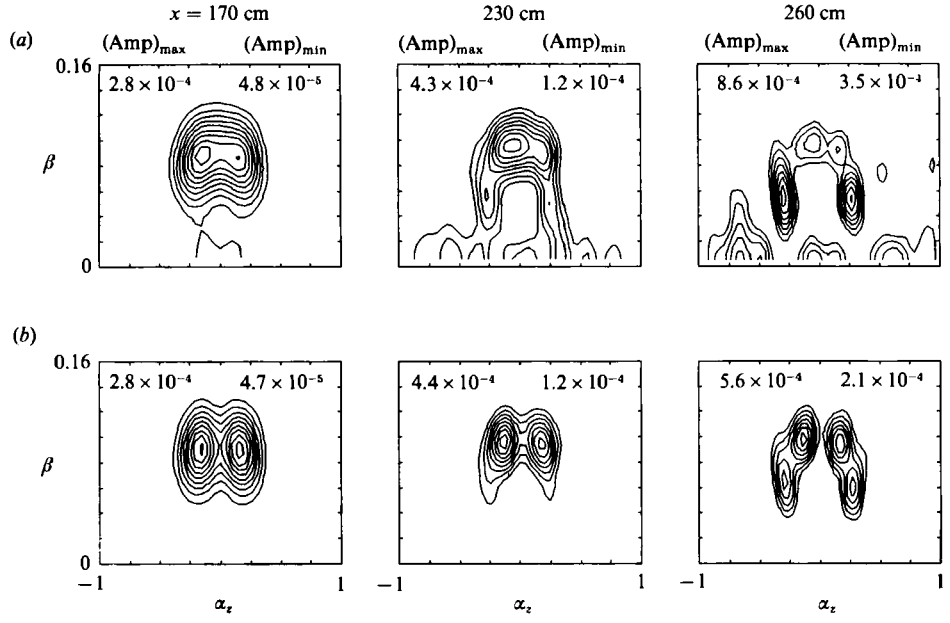

FIGURE 8. Spanwise wavenumber versus frequency spectra of (*a*) streamwise and (*b*) spanwise velocity fluctuation signals at $y/\delta_1 = 0.62$ and at three downstream locations representing the linear, subharmonic and post-subharmonic stages of the transition process.

local displacement thickness and Reynolds numbers have changed, the dimensional components of the wave packet evolve differently. For example, the dimensional frequencies of the most energetic oblique waves in the subharmonic stage are different in the two cases and do depend on the initial amplitude level. As in figure 4, we observed a post-subharmonic stage in which the formation of additional peaks of energy at approximately $\beta = 0$, $\alpha_z = 0$ and $\beta = 0$, $\alpha_z = \pm 0.7$. These peaks appear to be the result of nonlinear interactions involving the sums and differences of the primary and subharmonic peaks.

The spanwise structure of the disturbance at the three downstream stations representing the linear, subharmonic and turbulent stages of transition is shown in figure 9. At each downstream position the normalized streamwise and spanwise fluctuation velocities are plotted at 10 spanwise locations. The solid and dotted lines correspond to measurements obtained at positive and negative values of z respectively and at a y-location where $U/U_0 = 0.35$. Since the spanwise velocity is an antisymmetric function of the spanwise coordinate, the w-signal has been inverted when $z < 0$ for comparison purposes.

At the linear stage, the maximum amplitude of the u- and w-signals have approximately the same value. While the amplitude of the spanwise perturbation increases from zero at the centreline to a maximum at some distance away from the centreline and then decreases monotonically with increasing spanwise distance, the amplitude of the streamwise perturbation decreases almost monotonically with increasing distance from the centreline. However, it is possible that the streamwise fluctuation velocity might have an additional maximum away from the centreline at a different height in the boundary layer. By comparing the solid and dotted lines, it is demonstrated that the symmetry (and antisymmetry) of the disturbance is very good at the linear stage.

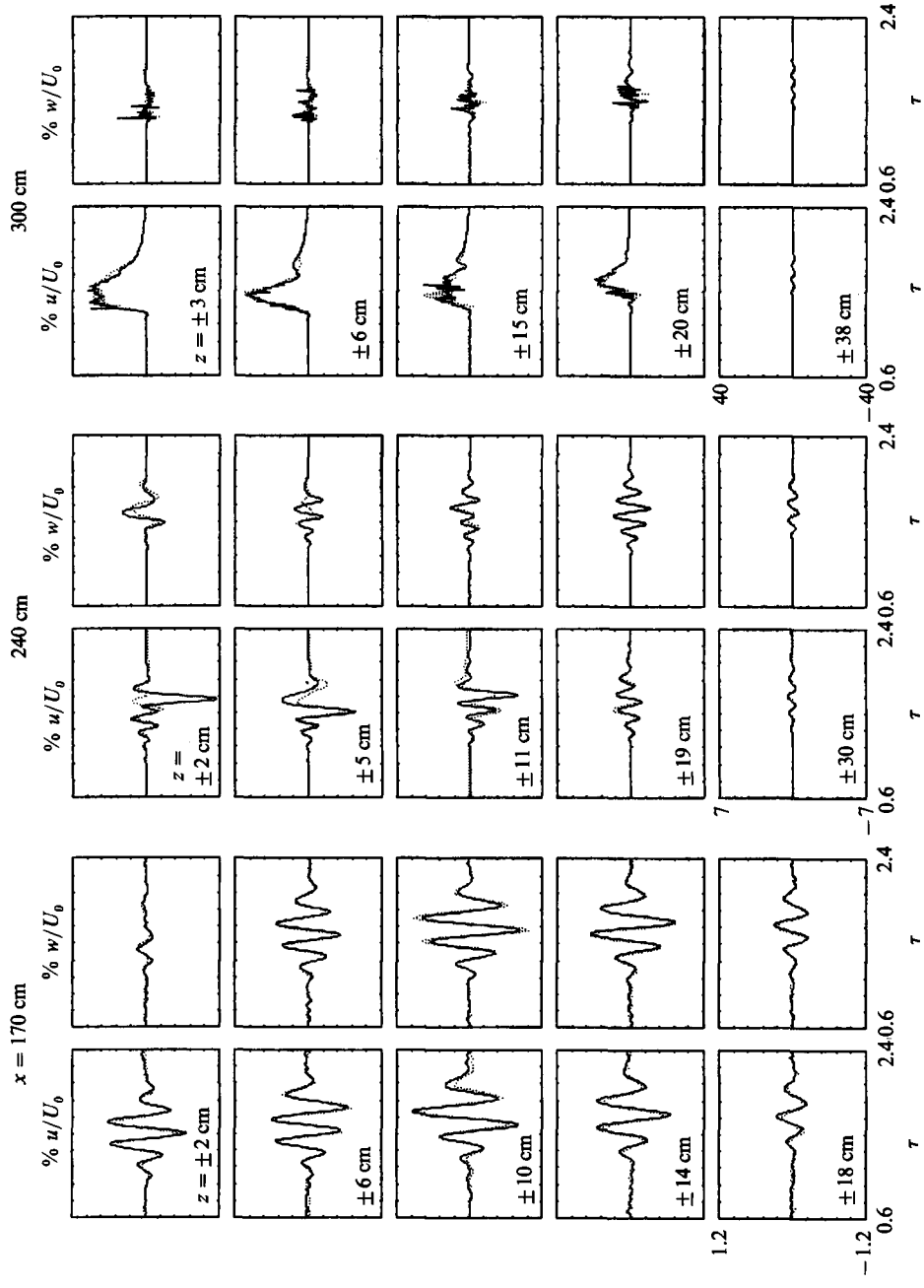

FIGURE 9. The spanwise structure of the wave packet at $y/\delta_1 = 0.62$ and at three downstream locations representing the linear, subharmonic and turbulent stages of transition are shown by a set of streamwise and spanwise velocity fluctuation records at various spanwise locations. The solid lines correspond to measurements obtained at positive z-values and the dotted lines correspond to values obtained at negative values of z (the w-component has been inverted to facilitate symmetry comparisons).

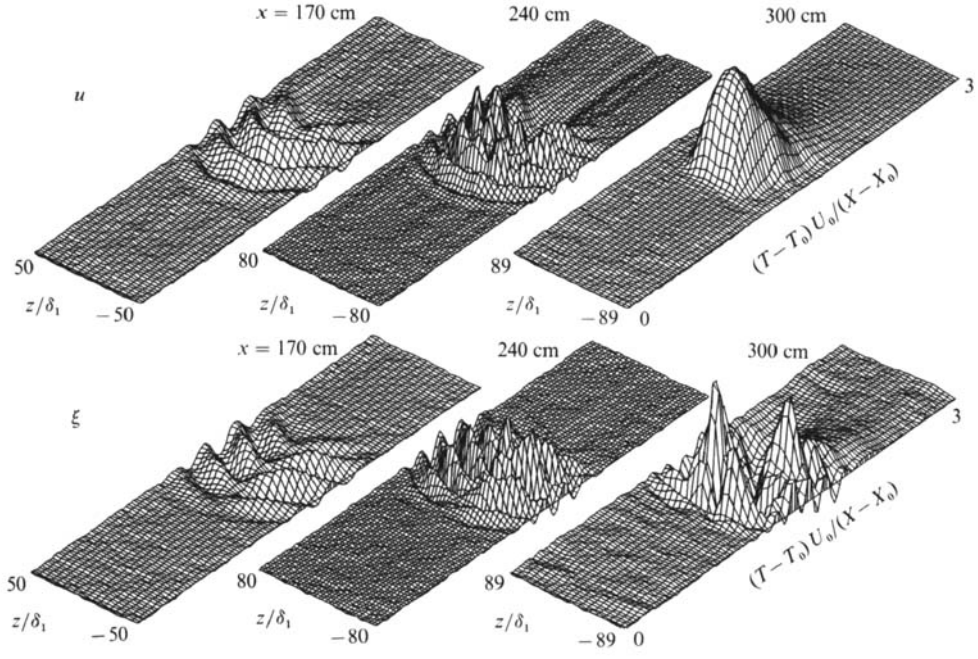

FIGURE 10. Perspective display of the streamwise velocity and vorticity fluctuations showing the different shapes of the wave packet at $y/\delta_1 = 0.709$ and at the three downstream locations representing the linear, subharmonic and turbulent stages of the transition process.

The symmetry of the disturbance structure is at its worst during the subharmonic stage. The symmetry is a strong function of the disturbance amplitude. As the distance away from the centreline increases, and the amplitude of the disturbance decreases, the signal recovers its 'linear' wave-packet form and its symmetry improves significantly. One possible cause for the loss of symmetry might have been a slight probe misalignment during data collection. Since the structure of the disturbance changes significantly with both y and z, a small error in the vertical or spanwise placement of the hot-wire probe would also result in an observed decreased spanwise symmetry. Close to the centreline where most of the nonlinearities take place (cf. §3.2), the amplitude of the streamwise signal is much larger than the amplitude of the spanwise perturbation velocity.

During the spot stage, the amplitude of the coherent spanwise velocity is negligible compared with the amplitude of the coherent streamwise fluctuations. Since there are, by this stage, significant turbulent fluctuations which are filtered out by the ensemble average, we cannot estimate the relative amplitudes of the instantaneous spanwise and streamwise components, only those of the phase-averaged components. However, both the u- and the w-velocities contain appreciable energy at high frequencies relative to what was observed in the linear and subharmonic stages. The spot manifests itself over a large spanwise range and far away from the centreline, at $z = \pm 38$ cm, the disturbance amplitudes are again small and the wave-packet shape still prevails.

The overall shape of the disturbance, at the linear, subharmonic and turbulent stages of transition and at a y-position where $U/U_0 = 0.4$, can best be seen in the perspective projections of the signal on the z-plane in figure 10. At the top of the figure, views of the streamwise velocity are shown representing the symmetric part

of the disturbance, while at the bottom of the figure views of the streamwise vorticity,

$$\xi = \frac{\partial w}{\partial y} - \frac{\partial v}{\partial z},$$

are shown, representing the antisymmetric portion of the structure. The streamwise vorticity records were computed from the flow field after the entire (y, z)-plane was mapped at the three representative downstream stations. The views shown in figure 10 represent the time history of the disturbance during its passage through a fixed downstream location. Note that the amplitudes shown at the three streamwise positions have been scaled differently. The wave character of the disturbance at $x =$ 170 cm is evident, while at $x = 240$ cm, the structure appears more complicated, and has achieved a turbulent-spot-like character by $x = 300$ cm. At this late stage, the high frequencies have lost their phase coherence and therefore, although the disturbance at $x = 300$ cm has a smooth appearance in figure 10, much information has been lost by the averaging. The structure at $x = 240$ cm is discussed in more detail in §3.3.

3.2. *Some theoretical considerations*

In the following section various experimental features observed and reported in §3.1 are discussed and explained in accordance with linear stability theory. The linear stage was modelled by Gaster (1975) who successfully reproduced the experimental results measured in collaboration with Grant (Gaster & Grant 1975) in which they followed the early development of the wave packet outside the boundary layer ($y/\delta_1 = 3.2$). In his analysis, Gaster assumed that the wave packet can be described as a superposition of the least-stable two- and three-dimensional waves which are the normal mode solutions of the Orr–Sommerfeld equation. Each fluctuating quantity, associated with a mode of non-dimensional frequency, β, and a spanwise wavenumber, α_z, can be expressed as

$$f = \hat{f}(y)\, \mathrm{e}^{\mathrm{i}(\alpha_x x + \alpha_z z - \beta t)}, \tag{1}$$

where α_x is a complex constant whose real and imaginary parts are the streamwise wavenumber and the growth rate respectively.

An important aspect, which is related to the linear stage and which needs further clarification, concerns the fact that the most amplified two-dimensional mode does not necessarily contribute the most energy to the u fluctuation velocity component.

For three-dimensional disturbances, the linearized equations of motion are the pair of equations (see Squire 1933; Benney & Gustavsson 1981)

$$\left(\frac{\mathrm{d}^4}{\mathrm{d}y^4} - 2k^2\frac{\mathrm{d}^2}{\mathrm{d}y^2} + k^4 - \mathrm{i}R\alpha_x\left[(\bar{U}-c)\left(\frac{\mathrm{d}^2}{\mathrm{d}y^2} - k^2\right) - \frac{\mathrm{d}^2\bar{U}}{\mathrm{d}y^2}\right]\right)\hat{v} = 0, \tag{2}$$

$$\left(\frac{\mathrm{d}^2}{\mathrm{d}y^2} - k^2 - \mathrm{i}R\alpha_x(\bar{U}-c)\right)\hat{\eta} = \mathrm{i}\alpha_z R\frac{\mathrm{d}\bar{U}}{\mathrm{d}y}\hat{v}, \tag{3}$$

where $k^2 = \alpha_x^2 + \alpha_z^2$, $c = \beta/\alpha_x$, and the phase velocity of the wave is given by $\beta/\mathrm{Re}\,(\alpha_x)$. R is the local Reynolds number based on the local displacement thickness and free-stream velocity.

Equation (2) is the familiar homogeneous Orr–Sommerfeld equation for the three-dimensional complex amplitude $\hat{v}$ of the vertical velocity v. The equation for the vertical vorticity amplitude, $\hat{\eta}$, is inhomogeneous and its homogeneous part has a different eigenvalue operator. While the structure of $\hat{v}$ depends only on the solution

of the Orr–Sommerfeld equation, the structure of the streamwise and spanwise fluctuating velocities depends on the solutions of both equations and is given by

$$\hat{u} = \frac{\mathrm{i}}{k^2}\left(\alpha_x \frac{\mathrm{d}\hat{v}}{\mathrm{d}y} - \alpha_z \hat{\eta}\right), \tag{4}$$

$$\hat{w} = \frac{\mathrm{i}}{k^2}\left(\alpha_z \frac{\mathrm{d}\hat{v}}{\mathrm{d}y} + \alpha_x \hat{\eta}\right). \tag{5}$$

Using Squire's (1933) theorem, we can relate any three-dimensional mode to an equivalent two-dimensional mode at a lower Reynolds number. We should emphasize that Squire's theorem does not guarantee that the two-dimensional mode is the most amplified mode. However, Watson (1960) showed in the temporal case for plane Poiseuille flow that below a threshold Reynolds number the two-dimensional mode is indeed the most amplified one, although for higher values of the Reynolds number (as one approaches the upper branch of the neutral curve) a three-dimensional mode can become the most amplified mode. At all values of the Reynolds number under discussion in this study, computations confirm that the two-dimensional mode remains the most amplified. Thus it is correct to state that the two-dimensional wave is the most amplified one and that it is the most energetic wave in terms of the normal fluctuations, v. However, for a given height in the boundary layer, it is not necessary that the two-dimensional mode be the most energetic wave in terms of the u-velocity component. While the magnitude of the streamwise two-dimensional mode depends only on $\hat{v}$ (since $\hat{\eta} = \hat{w} = 0$), the magnitude of a three-dimensional mode is a sum of contributions associated with both $\hat{v}$ and $\hat{\eta}$ (see (4)). This, however, is only true inside the boundary layer, since η goes to zero very rapidly outside the boundary layer where the mean shear, U', is zero (see (3)). In their experiments, Gaster & Grant (1975) placed their hot wire at $y/\delta_1 = 3.2$. This position lies outside the region of mean shear, and so their measurements reflect the contribution to u only from the Orr–Sommerfeld mode. As we shall show, the effect of η contributes to a marked contrast between the structure of the wave packet inside and outside the boundary layer.

The effect of η on the horizontal velocities is demonstrated in figure 11. The two-dimensional power spectra measured at $x = 170$ cm (linear stage) and at a y-location where U/U_0 is 0.5 are shown. The upper plots show the two-dimensional power spectra of the u and v velocity components measured with an $\times$-wire. The lower plots show the two-dimensional power spectra of the u and w velocity components measured with a V-shaped wire. It is evident that while the most energetic mode of the v velocity component is a two-dimensional wave, the most energetic mode of the u-component, due to the additional effect of the vertical vorticity, is a three-dimensional wave. It is also evident from the results presented in this figure that the use of the two different probes in measuring the streamwise fluctuation did not result in any significant difference.

The linear theory fails to predict the subharmonic stage, because it does not allow for the interaction between different modes. However, based on these measurements, it is believed that this stage can be described by wave-triad resonances based on the weakly nonlinear analyses of Raetz (1959, 1964), and Craik (1971). From figure 8 it is evident that most of the energy of the streamwise component of the wave packet is concentrated around two oblique waves and a single two-dimensional wave. The two oblique waves have a non-dimensional frequency of approximately 0.05 and spanwise wavenumbers of ± 0.276, while the non-dimensional frequency of the two-

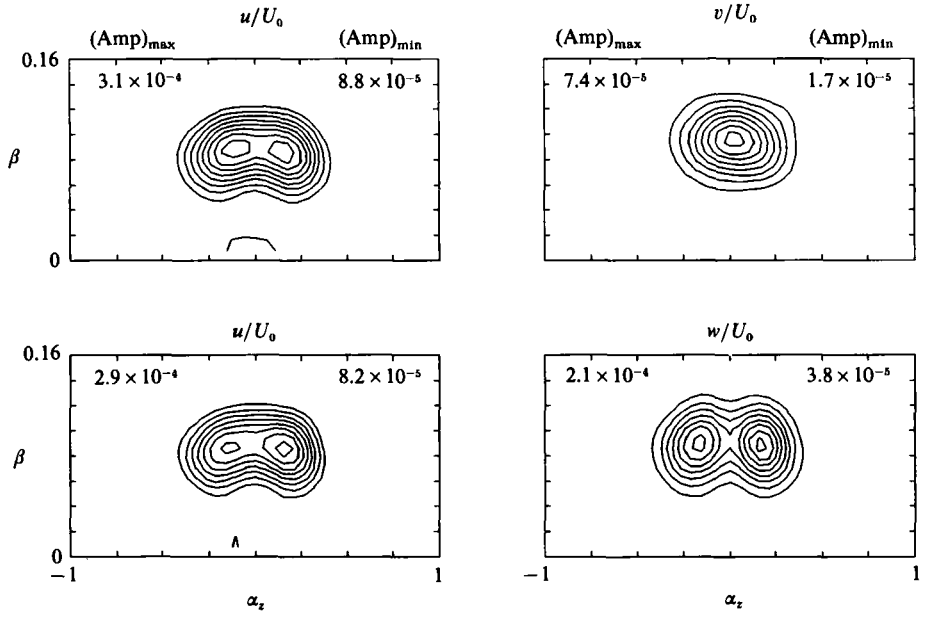

FIGURE 11. Linear stage, $x = 170$ cm, $y/\delta_1 = 0.897$. Spanwise wavenumber against frequency spectra of all velocity fluctuations showing that the most energetic mode is a two-dimensional wave only for the v-component. The top spectra were measured with an ×-wire while the bottom spectra with a V-shaped wire.

dimensional wave is about 0.1. The subharmonic resonance conditions for such a case require that the speeds of the two waves be the same, which implies that the axial wavenumber of the two-dimensional fundamental wave be twice as much as those of the subharmonic oblique waves. These conditions were verified by solving the Orr–Sommerfeld equation based on the local mean velocity profile and Reynolds number. The theoretical values for the streamwise wavenumber of the two-dimensional fundamental wave and the three-dimensional subharmonic wave were found to be 0.3 and 0.16 respectively, giving approximately the required ratio.

The resonance conditions are also fulfilled for the subharmonic stage shown in figure 4 at $x = 300$ cm associated with the first set of measurements. Moreover, the resonant conditions were also verified for a preliminary set of measurements where the free-stream velocity was 8 m/s and the wave packet was generated by oscillating vertically a small membrane located on the centreline of the plate at $x_0 = 50$ cm. At $x = 260$ cm the subharmonic wave had a non-dimensional frequency of 0.05 and spanwise and streamwise wavenumbers of 0.19 and 0.303 respectively.

At the two downstream stations representing the linear and subharmonic stages, measurements of all three velocity components were made, mapping the entire (y, z)-plane. A more detailed examination of the influence of the initial amplitude level of the wave packet on its spatial evolution was done by making dense measurements in the streamwise and spanwise directions and included a vertical mapping of the flow field which was absent in the first set of measurements. The flow was mapped at twelve vertical positions, nine inside the boundary layer where the local velocity (U/U_0) was $0.2, 0.3, \ldots, 0.9, 0.95$, and at three positions outside the boundary layer where y/δ_1 was 3, 4 and 5. At each height y, a double Fourier transform in time and the spanwise direction was carried out so that the vertical distribution for each mode could be obtained. The vertical amplitude and phase distributions of the most

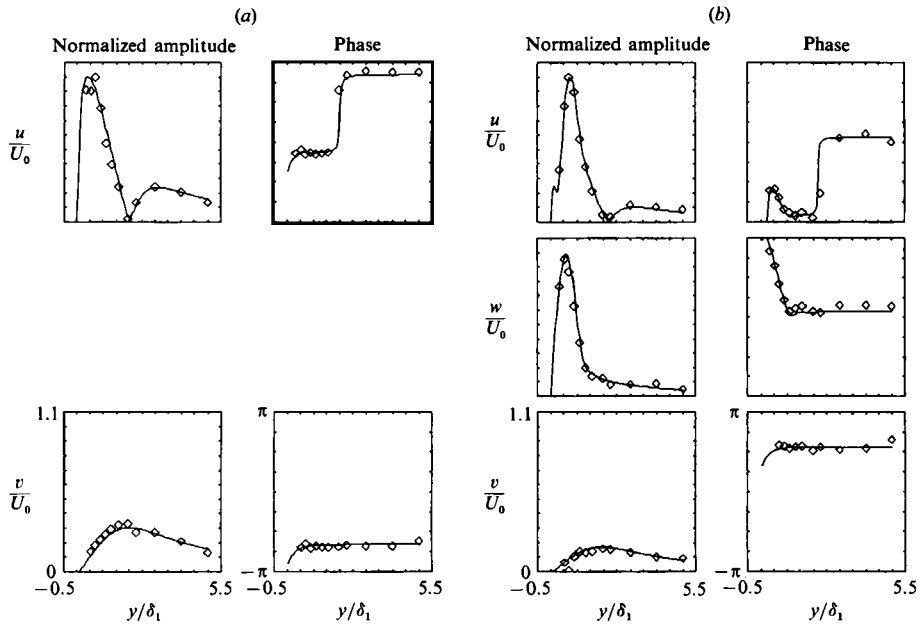

FIGURE 12. Linear stage, $x = 170$ cm. Comparison of measured and computed amplitude and phase distributions obtained for waves having (*a*) $\beta = 0.0859$, $\alpha_z = 0$, $(\alpha_x)_r = 0.258$, $(\alpha_x)_i = -0.0099$; (*b*) $\beta = 0.0859$, $\alpha_z = 0.16$, $(\alpha_x)_r = 0.246$, $(\alpha_x)_i = -0.0067$.

amplified two-dimensional wave, at the first of the downstream locations mentioned above, are shown in figure 12(*a*), while the distributions for a representative three-dimensional wave are shown in figure 12(*b*). The data points calculated from measurements are represented by the symbols while the solutions from linear stability theory are given by the solid lines.

It is important to emphasize that for each mode, only one free constant exists to match the amplitudes of all three velocity components. The constant was determined by matching the areas under the theoretically and experimentally obtained curves for the streamwise velocity components. In the comparison presented in figure 12 the streamwise velocity components were normalized to have a maximum of 1, and the vertical and spanwise components are scaled accordingly. In the comparison of the theoretical phase distributions with the measured ones, the measured phases were uniformly shifted by a constant to match the theoretical phase value at a given y-location.

The eigenvalue and eigenfunction solutions of the Orr–Sommerfeld equation (equation (2)) were obtained using a shooting method employing orthonormalization techniques (cf. Conte 1966). The solution of the vertical vorticity equation, (3), consists of homogeneous and particular parts. Davey & Reid (1977) proved that for a temporal amplification case (α_x real and β complex in (1)), the free spectrum of the vertical vorticity equation consists only of damped modes. This constraint was derived by multiplying the homogeneous part of (3) by the complex conjugate of $\hat{\eta}$ and integrating from $y = 0$ to infinity. By following the same procedure it can be easily shown that the same constraint holds for the spatial case (α_x complex, β real). In the present case the free spectra of (2) and (3) do not satisfy the resonance conditions given by Benney & Gustavsson (1981), and thus only the forced response to (3) determines the vertical vorticity structure.

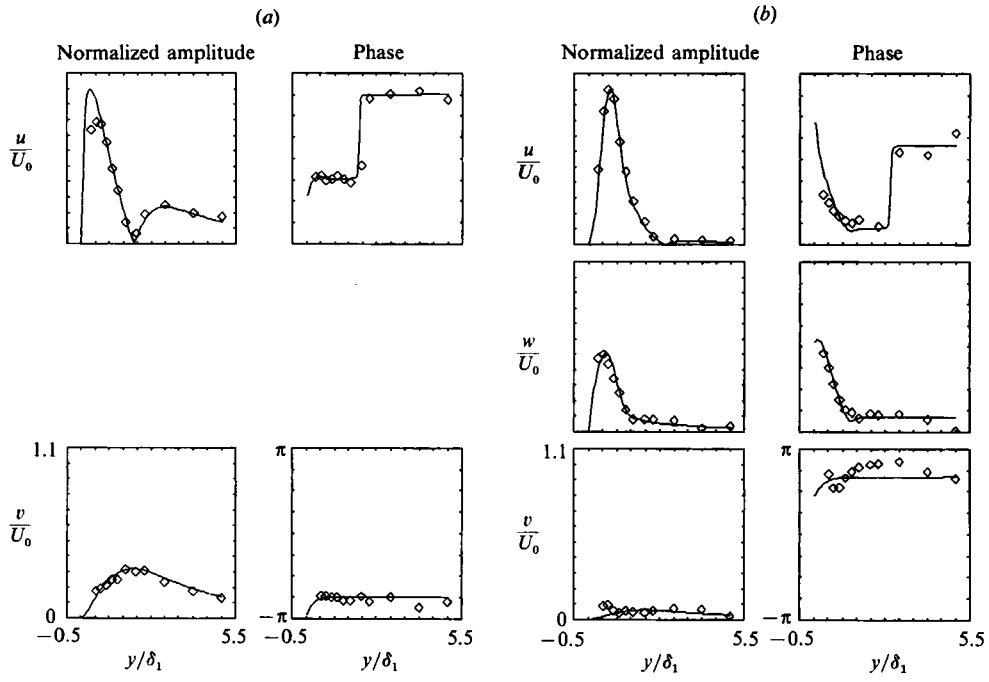

FIGURE 13. Subharmonic stage, $x = 240$ cm. Comparison of measured and computed amplitude and phase distributions obtained for waves having: (*a*) $\beta = 0.105$, $\alpha_z = 0$, $(\alpha_x)_r = 0.312$, $(\alpha_x)_i = -0.0025$; (*b*) $\beta = 0.052$, $\alpha_z = 0.23$, $(\alpha_x)_r = 0.145$, $(\alpha_x)_i = -0.0044$.

The amplitude and phase distributions at the linear stage are shown for the most amplified two-dimensional wave in figure 12(*a*), while the distributions corresponding to the most energetic mode in u, which is a three-dimensional wave, are shown in figure 12(*b*). The maximum values of the measured normalized streamwise fluctuation amplitudes of the two waves are 3.5×10^{-4} and 4.1×10^{-4}, respectively. The agreement between the theoretical and measured distributions is very good, but this is not too surprising, since the amplitude of the wave packet is still very small.

The amplitude and phase distributions at the subharmonic stage are shown in figure 13 for two waves participating in the subharmonic resonance. From the theoretical eigenvalues (given in the caption of figure 13) it is evident that the most energetic two-dimensional fundamental wave and its three-dimensional subharmonic wave, both propagate at almost the same phase velocity, thus fulfilling the resonance conditions. Although nonlinear mechanisms govern this stage, the agreement between the theoretical and measured distributions is quite good, suggesting the use of weakly nonlinear analysis in which the nonlinear terms of the equations of motion affect the growth of the amplitude with time and with downstream distance but do not affect the distribution of the disturbance along the shear coordinate y. There has been a considerable amount of work on the development and application of weakly nonlinear analysis in shear flows although most of the work has concentrated on the interactions between a single two-dimensional wave and a pair of oblique modes (for good reviews of the literature, see Craik 1985; Bayly, Orszag & Herbert 1988). The application of the theory to a wave packet has not (to our knowledge) been performed and is presently underway.

3.3. *The spatial structure of the disturbed flow*

The streamwise and vertical evolution of the disturbance shape can be seen from contour plots of the streamwise velocity component plotted in the (z,t)-plane in figure 14. Contour plots are displayed for two heights from the plate and for three downstream distances representing the linear, subharmonic and turbulent stages. The contours at the top and at the bottom of figure 14 correspond to measurements inside the boundary layer where $U/U_0 = 0.4$ ($y/\delta_1 = 0.709$), and to measurements outside the boundary layer where $y/\delta_1 = 4.0$. Initially, at the linear stage, the wave packet has an elliptic bowed shape and a wavy character which is emphasized by plotting contours having positive values with solid lines and contours having negative values with dotted lines. The wave packet outside the boundary layer has the same form as that inside the boundary layer except for a lower magnitude and a phase reversal of the entire structure. This is in accordance with the linear stability theory which assumes a superposition property and predicts the phase reversal and the decrease in magnitude of each normal mode outside the boundary layer (see figure 12).

At the subharmonic stage and inside the boundary layer the characteristic periodic structure within the packet is lost and warped wave fronts are formed having symmetrical maximum and minimum amplitudes on either side of the centreline. The contour plot of the wave packet outside the boundary layer does show the start of the peak splitting that seems to characterize the subharmonic stage, but the basic wave-packet shape is still present. The reason for this dramatic difference between what is observed inside the boundary layer and what is observed above the boundary layer is because the eigenfunction for the most energetic three-dimensional subharmonic mode (which represents the nonlinear interaction) goes to zero very rapidly outside the boundary layer (cf. figure 13). The explanation for this behaviour lies in the role of the vertical vorticity, η. Inside the boundary layer, the presence of a strong mean shear implies that the influence of η on the three-dimensional modes will be very strong (contributing as much as 80 % to the amplitude). However, above the boundary layer, where η is zero, only the Orr–Sommerfeld portion of u is present and hence the three-dimensional mode amplitude decreases significantly, and the disturbance retains its wave-packet shape. These results are in agreement with those of Gustavsson (1978) and Henningson (1988) who found that the horizontal velocities are dominated by η when a mean shear is present.

Figure 14 (and figure 10) show an apparent absence of wave structure at the turbulent spot stage. This is a result of the fact that the wavy structure present in any one such spot loses its phase coherence relative to another and consequently is averaged out by the ensembling process. However, the ensemble average still yields some relevant information concerning the low frequency and large-scale shape of the disturbance, and figure 14 indicates that a concentrated structure has formed with a single central maximum inside the boundary layer and a single minimum outside the boundary layer. At this downstream distance, the disturbance structure as a whole seems to have lost any resemblance to its original wave-packet shape.

The vertical structure of the disturbed region can be seen most readily from contour displays of the normalized streamwise velocity and vorticity fluctuations in the (y,z)-plane shown in figures 15–17. The displayed contours are shown for the three downstream distances representing the linear, subharmonic and turbulent stages. At each downstream station the contours are displayed for various passage times of the disturbance. The symmetrical part of the disturbance shape, represented

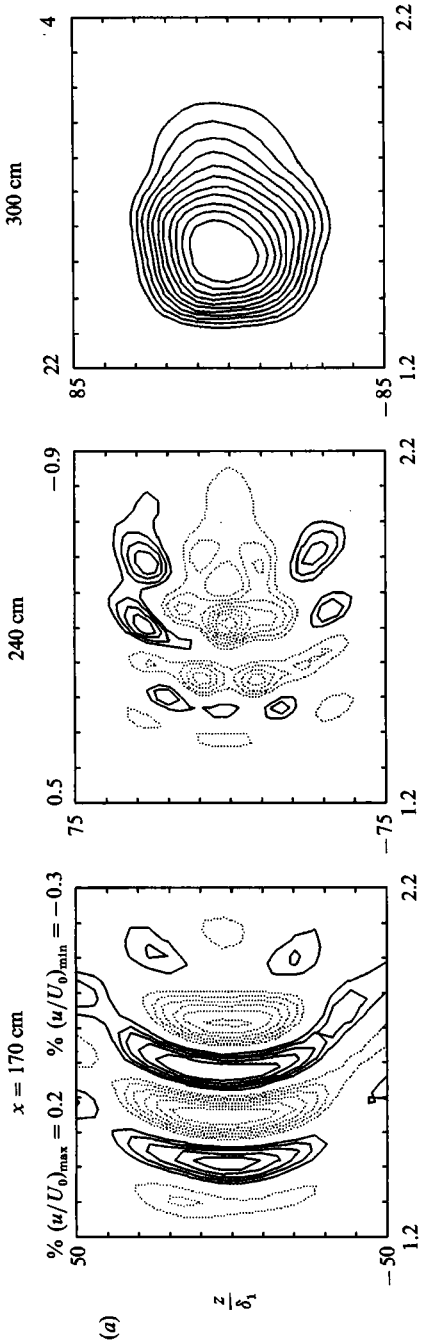

FIGURE 14. Contours of streamwise velocity fluctuation shown for the linear, subharmonic and turbulent stages of the transition and at (*a*) $y/\delta_1 = 0.709$ and (*b*) $y/\delta_1 = 4$. Solid lines represent positive contours, dotted lines represent negative contours.

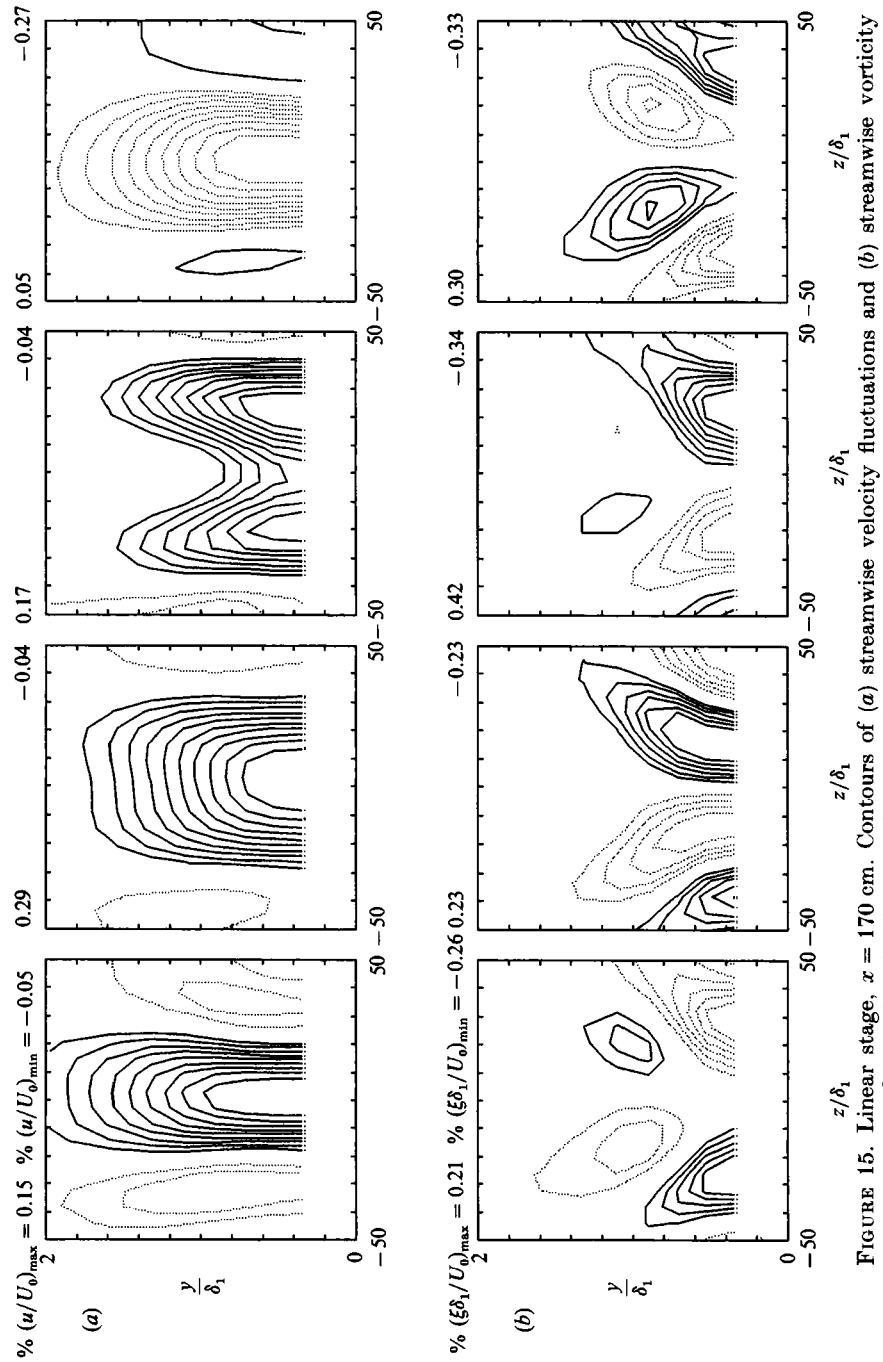

FIGURE 15. Linear stage, $x = 170$ cm. Contours of (*a*) streamwise velocity fluctuations and (*b*) streamwise vorticity fluctuations in the (y, z)-plane are shown at various passage times of the disturbance.

by contour displays of the normalized streamwise fluctuation velocity, is shown in part (*a*), while the antisymmetrical part, represented by contour displays of the normalized streamwise fluctuation vorticity, is shown in part (*b*). Positive and negative values are indicated by solid and dotted contour lines, respectively.

The wave-packet shapes at the linear stage are presented for various times in figure 15. The time parameter increases from left to right and covers a time range corresponding approximately to one half of a single period associated with the wave packet, as can be deduced by comparing the structures at $\tau = 1.405$ and at $\tau = 1.527$. Initially the streamwise velocity fluctuation has a single maximum located on the spanwise centreline and at a vertical distance corresponding approximately to the location where the most amplified wave attains its maximum according to linear stability theory. The vorticity structure consists of two major pairs of antisymmetric eddies (with respect to the spanwise centreline); the more intense pair is located closer to the centreline and above the weaker pair. As time increases, the concentrated u-structure broadens while the upper pair of streamwise vortices is amplified and moves towards the wall, 'pushing' the bottom pair outward. Then, the single peak of the u-structure splits into two on either side of the z-axis and a minimum peak between them is formed on the centreline. The spanwise locations of the two maximum peaks correspond to the spanwise locations of the maximum and minimum peaks of the streamwise vorticity eddies. Finally, a concentrated structure of negative streamwise velocity fluctuations arises around the location of the previous minimum peak and the entire structure of both u and ξ has a similar (but reversed) shape with respect to the structure formed initially.

The structure just described resembles the one inferred from streamlines only by Klebanoff *et al.* (1962). The streamline pattern at $\tau = 1.497$ resembles that corresponding to station C in their figure 19, while the disturbance shapes at the subharmonic stage, presented in figure 16 bear some resemblance to the structure corresponding to station D in the same figure.

While the structures of the streamwise vorticity fluctuations are similar to the structures shown for the linear stage, the shapes of the streamwise velocity fluctuations are more complicated at the subharmonic stage than at the linear stage. Initially, at $\tau = 1.466$, the streamwise velocity fluctuations exhibit a 'linear' shape similar to the one shown for the linear stage at $\tau = 1.497$, but the centre of symmetry is off the centreline. At $\tau = 1.497$ three symmetrical maximum peaks arise, and at the two resulting valleys between them, two minimum peaks are formed at a later time. Note that the spanwise wavelength of the vortical structure has been halved from what it was in the linear stage, similar to that observed by Klebanoff *et al.* (1962).

At the spot formation stage, shown in figure 17, the ratio between the normalized amplitudes of the streamwise velocity and vorticity fluctuations is an order of magnitude greater than the ratios observed in the previous stages. At the leading edge of the disturbance a concentrated structure extending outside the boundary layer and having negative values of streamwise velocity is formed. As the disturbance passes by, its amplitude increases and two peaks are formed; a positive peak very close to the wall and a negative one above it. The positive peak is strengthened while the negative peak is weakened until it becomes insignificant at later times. As mentioned above, the streamwise vorticity fluctuations are very weak, and the antisymmetry of their shape is poor.

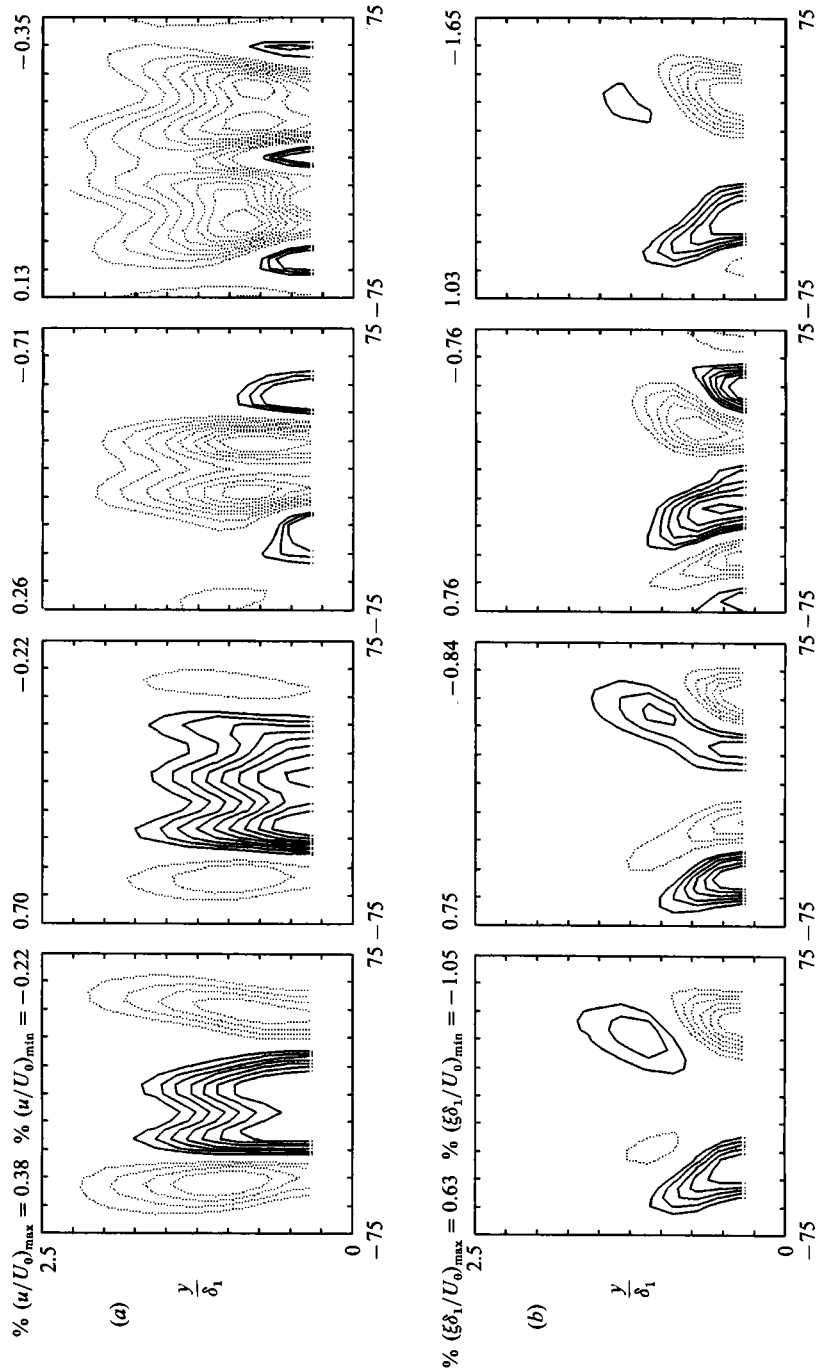

FIGURE 16. Subharmonic stage, $x = 240$ cm. Contours of (a) streamwise velocity fluctuations and (b) streamwise vorticity fluctuations in the (y, z)-plane are shown at various passage times of the disturbance.

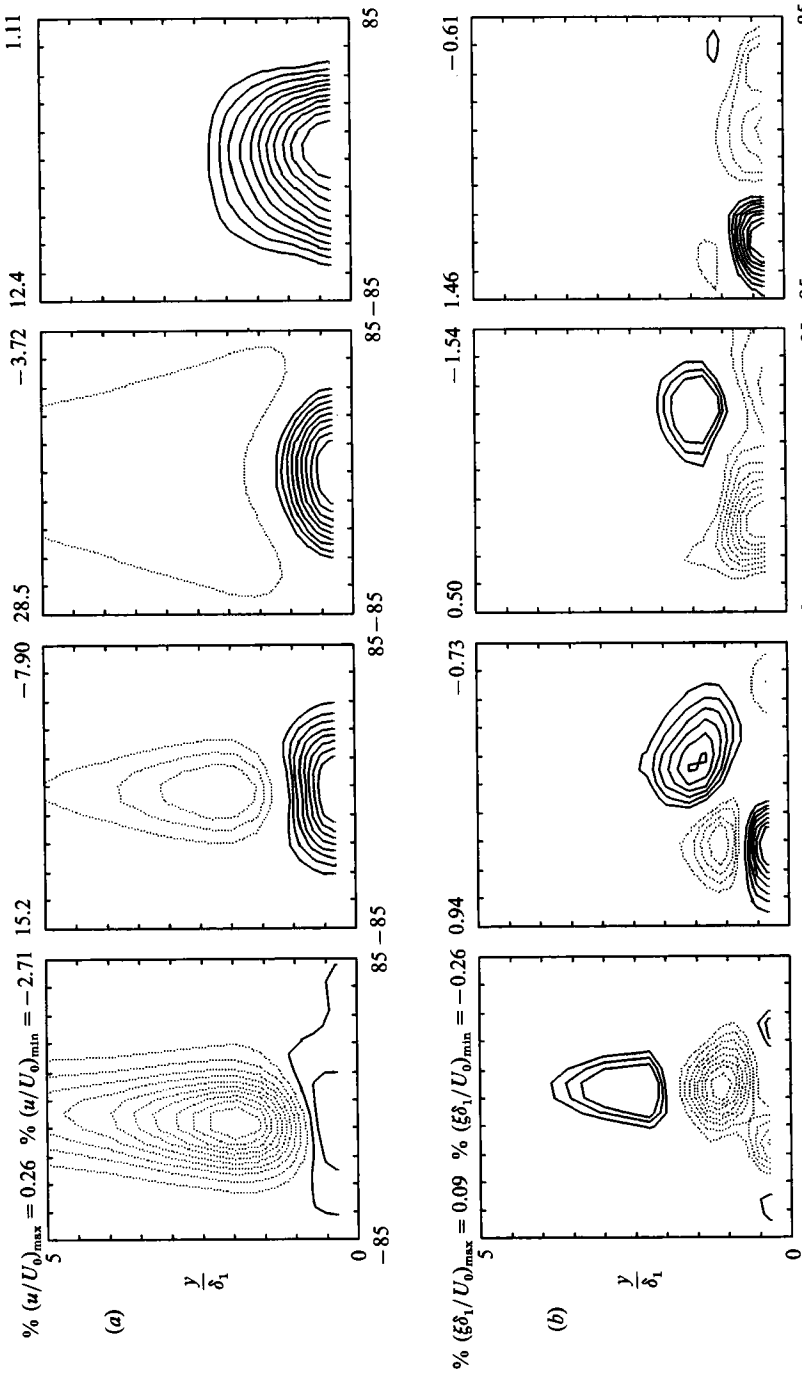

FIGURE 17. Turbulent stage, $x = 300$ cm. Contours of (*a*) streamwise velocity fluctuations and (*b*) streamwise vorticity fluctuations in the (y, z)-plane are shown at various passage times of the disturbance.

4. Conclusions

The evolution of a wave packet has been characterized as having three distinct stages. The linear stage agrees very well with the model proposed by Gaster (1975) and extends the measurements of Gaster & Grant (1975) to include the entire boundary layer. In the interior of the boundary layer, the effect of the vertical vorticity becomes important, and we find that owing to this, a three-dimensional mode becomes the most energetic wave in the streamwise velocity component, even though the two-dimensional mode is the most amplified according to linear stability theory. The second stage witnesses the growth of the subharmonic oblique mode which satisfies the three-wave resonance criterion for a Craik-type secondary instability. It should be emphasized that the subharmonic resonance is unforced, as it develops naturally. Although nonlinear interactions are very important in this stage, the eigenfunctions of each mode are still well predicted by linear stability calculations based on the local Blasius profile. In this stage, the role of the vertical vorticity is very dramatic and we see that the observations above the shear region reflect a very much simpler view of what is going on inside the boundary layer where the streamwise velocity fluctuations become dominated by the contribution of η.

The final stage of growth, the spot formation stage, starts with the growth of modes with high and low frequencies resulting from the sums and differences of the wavenumbers and frequencies of the two-dimensional fundamental and the three-dimensional subharmonic waves. After the establishment of this post-subharmonic stage, we see the rapid development of a broadband spectrum and a loss of coherence between the individual realizations. Only at this stage do we find significant distortion of the mean flow, indicating that the nonlinear interactions observed up to this stage are confined to the various components of the wave packet.

We would like to thank I. Wygnanski and M. Landahl for their contributions to this work and J. Olsson for repeating the detailed mean flow measurements. We are indebted to the Air Force Office of Scientific Research for support to J.C. under Contract F49620-83-C0019, without which the completion of this research would not have been possible. The assistance of the Bantrell Fellowship to J.C. is also gratefully acknowledged. K.S.B. was supported by the ONR Graduate Fellowship and also the Center for Fluid Mechanics at Brown University, supported by DARPA-URI grant N00014-86-K0754. J.H.H. enjoyed the support of ONR through grant N00014-90-J1302 during the preparation of this paper.

REFERENCES

Amini, J. & Lespinard, G. 1982 Experimental study of an "incipient spot" in a transitional boundary layer. *Phys. Fluids* **25**, 1743–1750.

Bayly, B. J., Orszag, S. A. & Herbert, T. 1988 Instability mechanisms in shear-flow transition. *Ann. Rev. Fluid Mech.* **20**, 359–391.

Benjamin, T. B. 1961 The development of three-dimensional disturbances in an unstable film of liquid flowing down an inclined plane. *J. Fluid Mech.* **10**, 401–419.

Benney, D. J. & Gustavsson, L. H. 1981 A new mechanism for linear and nonlinear hydrodynamic instability. *Stud. Appl. Maths* **64**, 185–209.

Benney, D. J. & Lin, C. C. 1960 On the secondary motion induced by oscillations in a shear flow. *Phys. Fluids* **3**, 656–657.

Breuer, K. S. & Haritonidis, J. H. 1990 The evolution of a localized disturbance in a laminar boundary layer. Part 1. Weak disturbances. *J. Fluid Mech.* **220**, 569–594.

BREUER, K. S. & LANDAHL, M. T. 1990 The evolution of a localized disturbance in a laminar boundary layer. Part 2. Strong disturbances. *J. Fluid Mech.* **220**, 595–621.

CONTE, S. D. 1966 The numerical solution of linear boundary layer problems. *Stud. Appl. Maths* **8**, 309–321.

CORKE, T. C. & MANGANO, R. A. 1989 Resonant growth of three-dimensional modes in transitional Blasius boundary layers. *J. Fluid Mech.* **209**, 93–150.

CRAIK, A. D. D. 1971 Nonlinear resonant instability in boundary layers. *J. Fluid Mech.* **50**, 393–413.

CRAIK, A. D. D. 1981 The development of wavepackets in unstable flows. *Proc. R. Soc. Lond.* A **373**, 457–476.

CRAIK, A. D. D. 1985 *Wave Interactions and Fluid Flows.* Cambridge University Press.

CRIMINALE, W. O. & KOVASZNAY, L. S. G. 1962 The growth of localized disturbances in a laminar boundary layer. *J. Fluid Mech.* **14**, 59–80.

DAVEY, A. & REID, W. H. 1977 On the stability of stratified viscous plane Couette flow. *J. Fluid Mech.* **80**, 509.

GASTER, M. 1968 The development of three-dimensional wave packets in a boundary layer. *J. Fluid Mech.* **32**, 173–184.

GASTER, M. 1975 A theoretical model for the development of a wave packet in a laminar boundary layer. *Proc. R. Soc. Lond.* A **347**, 271–289.

GASTER, M. 1982*a* Estimates of the error incurred in various asymptotic representations of wave packets. *J. Fluid Mech.* **121**, 365–377.

GASTER, M. 1982*b* The development of a two-dimensional wavepacket in a growing boundary layer. *Proc. R. Soc. Lond.* A **384**, 317–332.

GASTER, M. & GRANT, I. 1975 An experimental investigation of the formation and development of a wave packet in a laminar boundary layer. *Proc. R. Soc. Lond.* A **347**, 253–269.

GUSTAVSSON, L. H. 1978 On the evolution of disturbances in boundary layer flows. *Royal Institute of Technology, Department of Mechanics Rep.* Trita-Mek-78-02.

HENNINGSON, D. S. 1988 The inviscid initial value problem for a piecewise linear mean flow. *Stud. Appl. Maths* **78**, 31–56.

HERBERT, T. 1984 Analysis of the subharmonic route to transition in boundary layers. *AIAA Paper* 84-0009.

HERBERT, T. 1988 Secondary instability of boundary layers. *Ann. Rev. Fluid Mech.* **20**, 487–526.

ITOH, N. 1984 Landau coefficients of the Blasius boundary-layer flow. In *Turbulence and Chaotic Phenomena in Fluids* (ed. T. Tatsumi), p. 59. North-Holland.

ITOH, N. 1987 Another route to the three-dimensional development of Tollmien–Schlichting waves with finite amplitude. *J. Fluid Mech.* **181**, 1–16.

JORDINSON, R. 1970 The flat plate boundary layer. Part 1. Numerical integration of the Orr–Sommerfeld equation. *J. Fluid Mech.* **43**, 801–811.

KACHANOV, Y. S. & LEVCHENKO, V. Y. 1984 The resonant interaction of disturbances at laminar turbulent transition in a boundary layer. *J. Fluid Mech.* **138**, 209–247.

KLEBANOFF, P. S., TIDSTROM, K. D. & SARGENT, L. M. 1962 The three dimensional nature of boundary layer instability. *J. Fluid Mech.* **12**, 1–34.

LANDAHL, M. T. 1975 Wave breakdown and turbulence. *SIAM J. Appl. Maths* **28**, 735–756.

LANDAHL, M. T. 1980 A note on an algebraic instability of inviscid parallel shear flows. *J. Fluid Mech.* **98**, 243–251.

MORKOVIN, M. V. 1969 The many faces of transition. In *Viscous Drag Reduction* (ed. C. Wells). Plenum.

RAETZ, G. S. 1959 A new theory of the cause of transition in fluid flows. *Norair Rep.* NOR-59-383. Hawthorne, CA.

RAETZ, G. S. 1964 Current status of resonance theory of transition. *Norair Rep.* NOR-64-111. Hawthorne, CA.

SARIC, W. S. & THOMAS, A. S. W. 1984 Experiments on the subharmonic route to turbulence in boundary layers. In *Turbulence and Chaotic Phenomena in Fluids* (ed. T. Tatsumi), p. 117. North-Holland.

SCHLICHTING, H. 1933 Zur Entstehung de Turbulenz bei der Plattenströmung plattenstromung. *Nachr. Ges. Wiss. Göttingen*, 182–208.

SCHUBAUER, G. B. & SKRAMSTAD, H. K. 1947 Laminar boundary layer oscillations and stability of laminar flow. *J. Aero. Sci.* **14**, 69–78.

SQUIRE, H. B. 1933 On the stability for three-dimensional disturbances of viscous flow between parallel walls. *Proc. R. Soc. Lond.* A **142**, 621–628.

STUART, J. T. 1962 On three-dimensional non-linear effects in the stability of parallel flows. *Adv. Aero. Sci.* **3**, 121–142.

STUARTSON, K. & STUART, J. T. 1971 A non-linear instability theory of a wave system in plane Poiseuille flow. *J. Fluid Mech.* **48**, 529–545.

TOLLMIEN, W. 1929 Über die Entstehung der Turbulenz. *Nachr. Ges. Wiss. Göttingen*, 21–44 (transl. *NACA TM* 609).

WATSON, J. 1960 Three-dimensional disturbances in flow between parallel planes. *Proc. R. Soc. Lond.* A **254**, 562–569.